

SAND REPORT

SAND2003-0330

Unlimited Release

Printed January 2003

Compilation of Gas Intrusion Measurements, Variations, and Consequence Modeling for SPR Caverns

Thomas E Hinkebein

Prepared by
Sandia National Laboratories
Albuquerque, New Mexico 87185 and Livermore, California 94550

Sandia is a multiprogram laboratory operated by Sandia Corporation,
a Lockheed Martin Company, for the United States Department of
Energy under Contract DE-AC04-94AL85000.

Approved for public release; further dissemination unlimited.



Issued by Sandia National Laboratories, operated for the United States Department of Energy by Sandia Corporation.

NOTICE: This report was prepared as an account of work sponsored by an agency of the United States Government. Neither the United States Government, nor any agency thereof, nor any of their employees, nor any of their contractors, subcontractors, or their employees, make any warranty, express or implied, or assume any legal liability or responsibility for the accuracy, completeness, or usefulness of any information, apparatus, product, or process disclosed, or represent that its use would not infringe privately owned rights. Reference herein to any specific commercial product, process, or service by trade name, trademark, manufacturer, or otherwise, does not necessarily constitute or imply its endorsement, recommendation, or favoring by the United States Government, any agency thereof, or any of their contractors or subcontractors. The views and opinions expressed herein do not necessarily state or reflect those of the United States Government, any agency thereof, or any of their contractors.

Printed in the United States of America. This report has been reproduced directly from the best available copy.

Available to DOE and DOE contractors from

U.S. Department of Energy
Office of Scientific and Technical Information
P.O. Box 62
Oak Ridge, TN 37831

Telephone: (865)576-8401
Facsimile: (865)576-5728
E-Mail: reports@adonis.osti.gov
Online ordering: <http://www.doe.gov/bridge>

Available to the public from

U.S. Department of Commerce
National Technical Information Service
5285 Port Royal Rd
Springfield, VA 22161

Telephone: (800)553-6847
Facsimile: (703)605-6900
E-Mail: orders@ntis.fedworld.gov
Online order: <http://www.ntis.gov/ordering.htm>



SAND2003-0330
Unlimited Release
Printed January 2003

COMPILATION OF GAS INTRUSION MEASUREMENTS, VARIATIONS, AND CONSEQUENCE MODELING FOR SPR CAVERNS

Thomas E. Hinkebein
Underground Storage Technology Department
Sandia National Laboratories
P.O. Box 5800
Albuquerque, New Mexico 87185-0706

ABSTRACT

The intrusion of gas into oils stored within the SPR has been examined. When oil is stored in domal salts, gases intrude into the stored oil from the surrounding salt. Aspects of the mechanism of gas intrusion have been examined. In all cases, this gas intrusion results in increases in the oil vapor pressure. Data that have been gathered from 1993 to August 2002 are presented to show the resultant increases in bubble-point pressure on a cavern-by-cavern as well as on a stream basis. The measurement techniques are presented with particular emphasis on the TVP 95. Data analysis methods are presented to show the methods required to obtain recombined cavern oil compositions. Gas-oil ratios are also computed from the data and are presented on a cavern-by-cavern and stream basis. The observed increases in bubble-point pressure and gas-oil ratio are further statistically analyzed to allow data interpretation. Emissions plume modeling is used to determine adherence to state air regulations.

Gas intrusion is observed to be variable among the sites and within each dome. Gas intrusions at Bryan Mound and Big Hill have resulted in the largest increases in bubble-point pressure for the Strategic Petroleum Reserve (SPR). The streams at Bayou Choctaw and West Hackberry show minimal bubble-point pressure increases.

Emissions plume modeling, using the state mandated ISCST code, of oil storage tanks showed that virtually no gas may be released when H₂S standards are considered. DOE plans to scavenge H₂S to comply with the very tight standards on this gas. With the assumption of scavenging, benzene releases become the next most controlling factor. Model results show that a GOR of 0.6 SCF/BBL may be emissions that are within standards. Employing the benzene gas release standard will significantly improve oil deliverability. New plume modeling using the computational fluid dynamics code, FLUENT, is addressing limitations of the state mandated ISCST model.

Intentionally Left Blank

Contents		Page
1.0	Introduction	9
2.0	Gas Intrusion	11
2.1	Mechanism	11
3.0	Measurement Methods Using the Mini Skid/TVP 95	15
3.1	Presentation of Data Obtained with the TVP 95 and the Mini Skid	19
4.0	Statistical Analysis to Determine the Intrusion Rate for Each Cavern	21
4.1	Aggregation of Individual Cavern Data into Streams	22
5.0	The Compositional Analysis Methods of the TVP 95	27
6.0	Plume Analyses of Gaseous Emissions Using the ISCST Gaussian Dispersion Model	29
6.1	Single Tank Modeling - Assumptions and Approximations and Modeling Basis	30
6.2	Single Tank Model Results	31
6.3	Deliverability Based upon H ₂ S and Benzene Concentration	33
6.4	Discussion of Plume Modeling	35
7.0	Analysis of GOR Regain for Individual Caverns and Combined Streams	37
8.0	Conclusions	43
	Appendix A. Vapor Pressure History of Individual Caverns in the SPR	45
	Appendix B. Recombined Compositions of Oil Stored in SPR Caverns	55
	References	59

List of Figures	Page
Figure 1. Plot of gas flow into an SPR Cavern for salt matrix permeabilities of 10^{-20} , 10^{-21} , and 10^{-22} m ² .	12
Figure 2. Plot of time necessary to deplete a dome of 2-mile radius as a function of the average permeability of the salt matrix.	13
Figure 3. Schematic separator showing oil feed, F, off gas, G, and stabilized liquid, L.	15
Figure 4. The mini-skid oil separator consisted of two components.	15
Figure 5. The mini-skid separator consisted of the 40-gallon tank with manual control valves.	16
Figure 6. The trailer that contains the TVP 95 is completely mobile and self-contained.	16
Figure 7. The separator chamber for the TVP 95 is shown including the liquid level control float and a metal mesh to aid in gas-oil separation.	17
Figure 8. A view of the TVP 95 showing the separator, the computer used for control, and the gas chromatograph.	17
Figure 9. Sample output from the gas chromatograph.	18
Figure 10. Each downhole sampler has a volume of 10 liter.	19
Figure 11. The projected bubble points of the sweet streams at Bayou Choctaw.	24
Figure 12. The projected bubble points of the sour streams at Bayou Choctaw.	24
Figure 13. The projected bubble points of the sweet streams at Big Hill.	24
Figure 14. The projected bubble points of the sour streams at Big Hill.	24
Figure 15. The projected bubble points of the sweet streams at Bryan Mound.	24
Figure 16. The projected bubble points of the sour streams at Bryan Mound.	24
Figure 17. The projected bubble points of the sweet streams at West Hackberry.	25
Figure 18. The projected bubble points of the sour streams at West Hackberry.	25
Figure 19. Gaussian concentration distribution transverse to flow.	29
Figure 20. Plots of H ₂ S concentration in a 100 MSCF/hr plume.	32
Figure 21. Cumulative distribution of wind speed for Port Arthur in 1992.	33
Figure 22. Emissions of H ₂ S deliverability of oil at 30 MBH (30,000 BBL/hr).	34
Figure 23. Emissions of benzene for deliverability of oil at 30 MBH.	35
Figure 24. Projected GOR rate increase brackets showing average increase rate and + 2 σ for Bayou Choctaw at the delivery temperature of 90°F.	39
Figure 25. Projected GOR rate increase brackets showing average increase rate and + 2 σ for Bayou Choctaw at the delivery temperature of 90°F.	39
Figure 26. Projected GOR rate increase brackets showing average increase rate and + 2 σ for Big Hill at the delivery temperature of 95°F.	39
Figure 27. Projected GOR rate increase brackets showing average increase rate and + 2 σ for Big Hill at the delivery temperature of 95°F.	39
Figure 28. Projected GOR rate increase brackets showing average increase rate and + 2 σ for Bryan Mound at the delivery temperature of 90°F.	40

	Page
Figure 29. Projected GOR rate increase brackets showing average increase rate and + 2 σ for Bryan Mound at the delivery temperature of 90°F.	40
Figure 30. Projected GOR rate increase brackets showing average increase rate and + 2 σ for West Hackberry at the delivery temperature of 90°F.	40
Figure 31. Projected GOR rate increase brackets showing average increase rate and + 2 σ for West Hackberry at the delivery temperature of 90°F.	40
Figure 32. A comparison between the gas-oil ratio and the bubble point pressure for all vapor pressure data.	

List of Tables	Page
Table 1. Standard Deviation for Individual Cavern Historical Intrusion Rates at 100 °F	22
Table 2. Blended Stream Intrusion Rates and Standard Deviation of Average Intrusion Rate	23
Table 3. Cavern gas-oil ratios, GOR increase rates, and measurement uncertainty as analyzed at 100 °F.	38
Table 4. Stream averages of the GOR, its increase rate, and statistics.	39

1.0 Introduction

The United States Strategic Petroleum Reserve (SPR) is currently (August, 2002) storing approximately 580 million barrels of crude oil to buffer shortfalls in foreign supply oil. This oil is stored in 62 underground solution mined (leached) caverns. These caverns are located approximately 2000 to 4000 feet below the earth's surface in salt domes. Subsurface caverns, as opposed to other types of storage, were selected for storage because of their ease of construction (solution mined), low cost, and their impermeability to oil penetration, thus ensuring long-term integrity for the stored oil.

While there are many advantages to oil storage in salt domes, there are some disadvantages. Foremost among these are factors that cause the vapor pressure of the stored oil to increase. The first of these factors is the heating of cavern fluids in response to geothermal effects. For most caverns within the SPR, the salt temperature due to the geothermal gradient at the cavern midpoint is 120 – 130 °F. As the temperature of the oil increases, the vapor pressure also increases in all caverns in a very predictable manner. Because the SPR receives oil at 80°F and can, according to the Level 2 Design Criteria, cool oil to 90°F using raw water temperatures, thermally induced vapor pressure rise is responsible for the major increase in the vapor pressure of the stored oil. At times during the year, greater or lesser cooling is possible. Over and above the thermal effects, the second cause of vapor pressure rise is the absorption of gases by the stored oil.

There are several sources of gas to be considered:

1. Most gas associated with oil production is removed at the wellhead. In some cases, there is a small residual of gas in the oil.
2. When oil is shipped in oil tankers, inerting atmospheres of nitrogen and carbon dioxide assure that oil arriving at U.S. ports is stable at approximately 70 – 80 °F and 1 (one) atmosphere of pressure.
3. When the oil is stored in caverns, the oil may absorb dissolved nitrogen and oxygen from the water/brine used as the cavern transfer fluid.
4. Nitrogen derived from cavern integrity testing is also transferred to the oil.
5. Interstitial gases trapped in the salt may be released in leaching and transferred to the oil.
6. Occluded gases of methane, carbon dioxide, nitrogen, and light hydrocarbons are also transferred from the salt to the oil.

While oil is stored in caverns, there is no problem associated with increasing vapor pressure because the storage pressure greatly exceeds the vapor pressure. However, upon movement of oil out of the caverns, the oil is typically transported to tanks. When oil is stored in tanks, the confining pressure is atmospheric. If the vapor pressure of the oil is greater than the atmospheric pressure, then off gassing occurs. This oil is called gassy oil. Off gassing can lead to the release of gases that are detrimental to the environment, health and safety. These gases include propane, benzene and H₂S. The amount of off gassing allowed is governed by safety and environmental regulations. Hence, it is important to know the vapor pressure of stored oil.

Since 1995, the measurement of vapor pressure of crude oils stored in the SPR has been determined using the TVP 95. This device was invented and built to measure the vapor pressure of low vapor pressure oils that have been discovered in caverns within the reserve. This device consists of a flow-through gas-oil separator that is operated with a closed vapor space and a continuously flowing oil stream. Once steady state is obtained, the pressure in this device corresponds to the oil bubble point.

A different way of gauging the oil vapor pressure is to measure the gas-oil ratio at atmospheric pressure. With the TVP 95, the GOR measurement is accomplished by allowing the gas stream to escape from the separator. The flow rate of the gas stream is determined to provide a direct measure of gas-oil ratio. The TVP 95 affords the SPR a reasonably accurate (plus or minus 14% as determined from repeated measurements on the same cavern) and consistent method of determining the oil vapor pressure.

In addition to vapor pressure measurements, another focus of the sampling program is to determine the composition of the stored oil. When the TVP 95 analyzer is used, the composition of the vapor space is always determined. These data are then analyzed using the Soave-Redlich-Kwong, SRK, equation of state without interaction coefficients to allow the greatest compatibility with standard process simulators. Results from this analysis give us the composition of the light fraction of the crude oil stream. This compositional analysis gives us some insight into the nature of the intruding gas.

By gathering these data over an extended period of time, regain rates, or vapor pressure increase rates, for each cavern can be predicted. The regain rate is defined as the rate of vapor pressure increase as a function of time. These regain rates vary greatly from cavern to cavern. Additionally, it has been observed that the various SPR sites have very different regain rates. The SPR Bryan Mound and Big Hill storage sites have the greatest regain rates while West Hackberry and Bayou Choctaw have smaller regain rates. Because of the number of caverns involved and the relative difficulty of obtaining samples, the number of data points for each cavern is usually quite small so that the uncertainty in the data is large. Recently, increases in the sampling frequency at all locations have improved this situation. This frequency increase will lead to more accurate estimates of the regain for each cavern.

Lastly, the effects of off gassing are analyzed using plume studies. When gassy oil is transferred to storage tanks, off gassing occurs. The off gas may then be carried by the wind in an air plume. Analysis of this plume is necessary to ensure compliance with environmental and safety regulations. H₂S is the most critical gas released by sour and sweet crude oils. Benzene is another compound requiring critical attention. Atmospheric dispersion modeling of emitted gases allows us to determine critical amounts of gas that may be released and the concentrations that will develop in proximity to a storage tank.

This report will consider observations of gas intrusion, the measurement methods used, the analysis methods, and the consequences of gaseous release. The measurement methods will be described as well as the analysis methods to obtain compositional information. Plume modeling and consequence modeling will also be presented.

2.0 Gas Intrusion

Six potential sources of gas absorption were mentioned in the last section. These sources are:

1. Produced gases;
2. Inerting gases;
3. Gases dissolved in water or brine and subsequently transferred to the oil phase;
4. Nitrogen derived from cavern integrity testing;
5. Interstitial gases in the salt and released to the cavern by leaching; and
6. Interstitial gases which permeate through the salt to the oil phase.

All of these gas sources may be operating and can lead to increases in the oil vapor pressure. A little more may be said about each mechanism. The first two mechanisms are observed to occur before cavern storage and is responsible for raising the vapor pressure of the oil to atmospheric conditions.

The third mechanism, of gases from brine, can and does occur in all caverns and is operating at gassy sites (Bryan Mound and Big Hill) as well as non-gassy sites. Judging from calculations of source term size and the response of cavern vapor pressure at non-gassy sites, this mechanism is probably most important during initial cavern fill. It is probably responsible for an up to 2 psi increase in oil vapor pressure.

The fourth mechanism is nitrogen absorption from cavern integrity testing. This mechanism is responsible for elevating the vapor pressure of oil stored at the tops of caverns. It is not known how extensive this contamination is, but the effect can be very misleading when trying to determine the amount of vapor pressure rise for the bulk of the cavern oil. Since the least expensive sampling method is to flow oil out of the top of a cavern, the type of contamination will most affect the results when this sampling method is used.

The last two mechanisms involve gas intrusion from the salt itself. A number of gases occur naturally in domal salts. The amount of these gases is highly variable between domes with some having small amounts of gas and others having larger amounts of gas. These gases include methane, nitrogen, carbon dioxide, and light hydrocarbons. Gases collect at salt grain boundaries as well as in pockets in the salt. These gases are presumed to exist at lithostatic pressure. When a cavern is leached in the salt, it sometimes intercepts these pockets of gas causing the gas to be immediately released to the fluid. After a cavern is created, these gases also migrate into the cavern as a result of the natural permeability of salt. Ehgartner, Neal and Hinkebein [1998] have studied gas releases from salt in some detail. In the next section, we will consider the mechanisms of gas intrusion.

2.1 Mechanism

The mechanism to describe gas intrusion into a salt storage cavern has never been directly measured or positively formulated. Instead we must rely upon measurements of

vapor pressure rise and surmise the cause of the increase. The available measurements do not establish cause but rather indicate whether a mechanism is plausible. Further, logical information about the regain is employed to assist in the determination of appropriate mechanisms.

Ehgartner [1993] has suggested that the primary mechanism by which gas enters a cavern is diffusion from permeable salt [Hinkebein et al., 1995]. Ehgartner found that a value for the permeability of 10^{-21} m^2 over the complete cavern surface area produced reasonable values of gas intrusion as shown in Figure 1. In this analysis, the permeable flow is driven presumably by the force difference between gas pockets at lithostatic pressure (3000 psi at 1 psi/ft) and cavern hydrostatic pressure (1600 psi) or approximately 1400 psi at mid-cavern depth. Cummingham and Williams [1980] question the mechanism of permeability as the pore size approximates the molecular size. They use the term configurational diffusion to describe the movement of mass through extremely small pores.

Prior to the first round of degassing, oil had been stored in SPR caverns for approximately 20 years. At that time, the average GOR of oil was approximately 3 SCF/BBL but was highly variable. This amount of gas intrusion matched reasonably well with a salt matrix permeability of 10^{-21} m^2 . As is shown below, however, other factors do not completely support this mechanism.

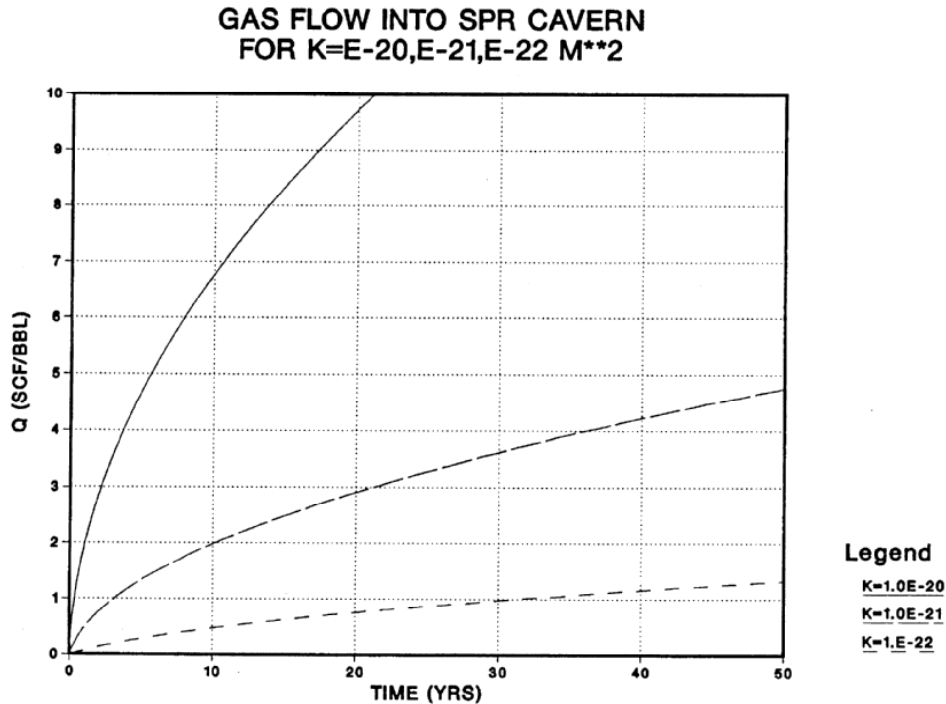


Figure 1. Plot of gas flow into an SPR Cavern for salt matrix permeabilities of 10^{-20} , 10^{-21} , and 10^{-22} m^2 . The total amount of gas intrusion, Q, is measured in SCF of intruding gas per barrel of oil in a cavern. Note that Q is less than the gas-oil ratio because the intruding gas will strip other gases out of the oil as a consequence of dropping the pressure during the measurement of GOR.

The determination of the true salt permeability is limited by the experimental methods used to make the measurements. By-pass leakages have tended to limit the lowest values that the equipment can measure. Thus, the measurement of the true salt permeability has been continuously decreasing over time as equipment and methods have improved. Older measurements [Bauer, 1993] of salt permeability have shown values to be approximately 10^{-14} to 10^{-16} m^2 . As techniques have improved, however, these values have steadily decreased as leakage around the salt cores is minimized. By 1990, measurements of salt permeability were 10^{-18} to 10^{-21} m^2 . Indeed, the true permeability of undisturbed salt has an unknown value that may approach the values corresponding to the salt mass diffusivity. Yet the presence of the caverns disturbs the salt surrounding the caverns, and the resulting stresses can increase the permeability.

Another paradox related to the permeable intrusion of gas is as follows: If the salt is permeable, why is any gas left in the dome? Our geologic understanding of the Gulf Coast salt domes is that they are about 50 million years old (± 10 to 15 million years). It is further believed that gas trapped in the salt is at lithostatic pressure while off dome gases are presumed to exist at hydrostatic pressure. If we use the same permeability model as was used to develop Figure 1, we find the total depletion of gas from the dome as presented in Figure 2. From this figure, we see that all of the overpressured gas in the dome is bled down to hydrostatic pressure at 10 million years when the salt permeability is 10^{-21} m^2 . If the permeability were smaller than this value, not enough gas permeates into caverns to explain the gas intrusion phenomenon shown in Figure 1. It is thus concluded that if the uniform permeability model were completely correct, there would have been no gas to intrude into the caverns.

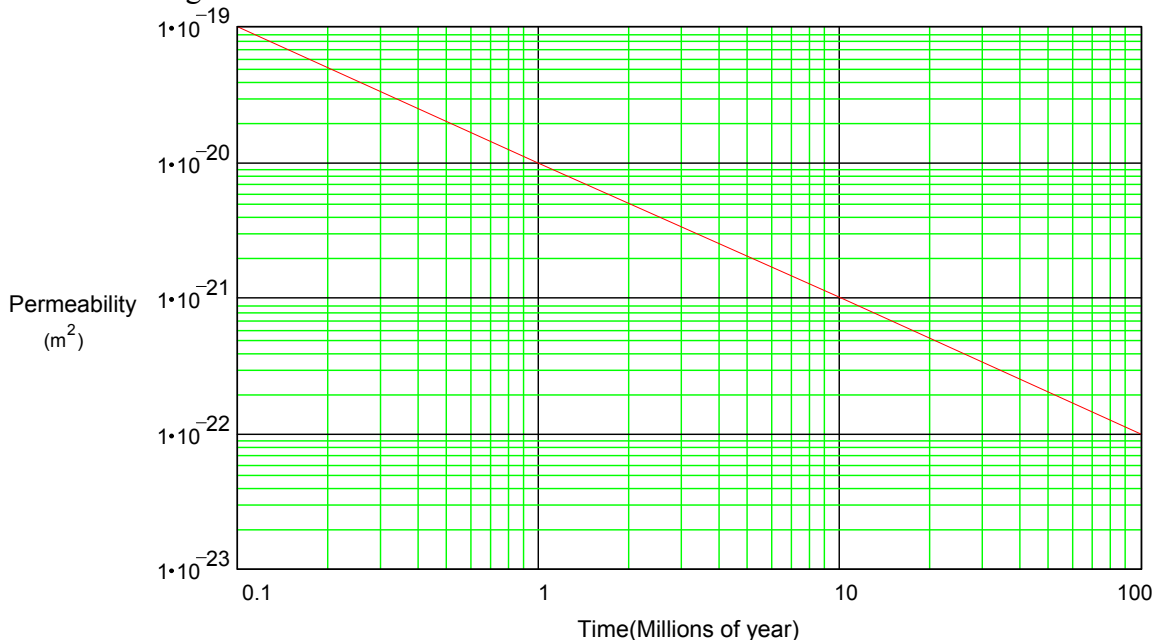


Figure 2. Plot of time necessary to deplete a dome of 2-mile radius as a function of the average permeability of the salt matrix.

Alternate permeability intrusion mechanisms have been proposed. One of the options is that the bulk of the salt is completely impermeable and that it is laced with permeable zones. Another option is that salt damage near each cavern is responsible for enhanced permeability in that area. This enhanced permeability leads to the slow depletion of gas zones in the vicinity of the cavern. Stormont (2002) has explored the impact of a near cavern disturbed rock zone on the permeability of salt near each cavern. Enhanced permeability near a cavern would explain intrusion of gas without depleting all of the gas in the dome. One other factor supporting a permeability mechanism is a very weak dependence for gas intrusion on the cavern operating pressure (Hinkebein et al, 1995). Applying a higher back pressure on the salt face does result in a small decrease in gas intrusion.

Leaching also releases gas from the salt. Estimates of the gas-filled porosity in salt deposits vary from 1 to 5%. In relatively pure domal salt, the gas-filled porosity is typically less than 0.4%. This porosity may be gas filled or gas saturated brine filled. (Iannacchione et al., 1982) This mechanism of gas intrusion was also analyzed in Hinkebein et al., 1995. When salt is dissolved, gas trapped in pockets and along grain boundaries is released. During the initial leaching of a cavern, this gas is released into the water phase. Most of the released gas is circulated out of the cavern with the disposed brine. A limited amount of gas is concentrated in the roof oil and may later be redistributed to the complete cavern inventory through convective mixing driven by the geothermal gradient in the domal salt.

On the other hand, when oil is circulated out of the cavern by the addition of freshwater, newly released gas will be concentrated in the oil phase. Within any cavern, there is enough circulation of oil and brine in caverns that a chemical equilibrium between the phases is presumed. For this case at typical cavern operating conditions, the chemical equilibrium between oil and brine dictates that the concentration of methane in the oil phase is 700 times the concentration of methane in the brine phase. This process can result in significant increases in the oil vapor pressure. These increases in oil vapor pressure will be observed subsequent to the freshwater addition. This mechanism suggests that gas intrusion may be a function of operation, i.e., fresh water movement and not time.

Based on current data it is impossible to tell which of these alternate explanations has the most merit. From the standpoint of measured bubble point increase, the most important fact is that the bubble point is increasing! We will endeavor to discover the mechanism of gas intrusion, but this process will be secondary to the primary mission of accurately determining intrusion rates.

3.0 Measurement Methods Using the Mini Skid/TVP 95

The determination of the oil vapor pressure has been primarily accomplished by using a benchscale oil-gas separator. This measurement method is depicted schematically in Figure 3.

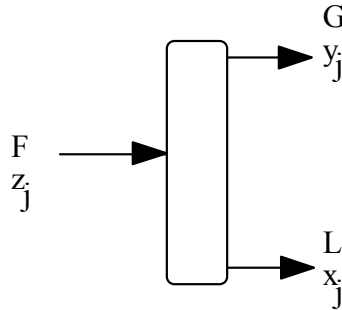


Figure 3. Schematic separator showing oil feed, F , off gas, G , and stabilized liquid, L . The symbols, x_j , y_j , z_j , represent the compositions of the liquid, gas, and feed streams.

Upon entering the separator, gas is evolved. Measurements are made of all of the individual flow rates as well as the composition of the gas stream leaving the separator. When the outlet gas valve is open, gas is evolved at atmospheric pressure, and the gas-oil ratio, GOR, is measured. When the gas flow valve is shut, the separator moves to a steady state pressure, and this pressure is the bubble point.



Figure 4. The mini-skid oil separator consisted of two components. The temperature control tank is on the left while the separator is shown on the right.

The original separator is shown in Figures 4 and 5. In Figure 4, several vessels are shown. The one on the left is a temperature control tank that is used to adjust the temperature of the oil to approximately 100 degrees Fahrenheit. From there, oil flows to the separator shown in Figure 5. Both oil and gas flow rates are measured in addition to the gas composition. Direct measurements of the bubble point are obtained by closing the gas exit valve. The steady-state pressure obtained as oil continues to flow, but with the vapor phase shut-in, is the bubble-point pressure. Manual control of the separator

was required to keep the liquid level, flow rates, temperatures and pressures constant. While this process was tedious, it produced unbiased results for the oil vapor pressure. At least three people were required to operate the mini skid.



Figure 5. The mini-skid separator consisted of the 40-gallon tank with manual control valves and a site glass to monitor the liquid level.

In 1995, the measurement process was partially automated with the construction of the TVP 95 by Pencor Laboratories. The trailer for this device is shown in Figure 6. This measurement device was completely mobile and self-contained. The automation of the TVP 95 included complete control of the incoming oil temperature, flow rates, and liquid level in the newly designed separator as shown in Figure 7. The separator consisted of a glass tube to allow visualization of the separation process. A metal mesh aided the separation of gas from the oil. An internal float interfaced with computer control to allow liquid level to be automatically controlled. At steady state, the pressure for the confined vapor equilibration is equal to the bubble point.



Figure 6. The trailer that contains the TVP 95 is completely mobile and self-contained.



Figure 7. The separator chamber for the TVP 95 is shown including the liquid level control float and a metal mesh to aid in gas-oil separation. The separator is enclosed in a thermostatically controlled chamber. The separator is made of glass and the front of the controlled chamber is made of Plexiglas so that separation may be observed.

Figure 8 shows a complete picture of the working TVP 95. The computer controlling the process operates with the LabVIEW program. The gas chromatograph is used to analyze samples of the vapor phase. In Figure 9, an example of a gas chromatograph output is presented. The area under each peak is directly proportional to the amount of that component in the gas. In this way, the total gas release is speciated into the individual components.



Figure 8. A view of the TVP 95 showing the separator, the computer used for control, and the gas chromatograph.

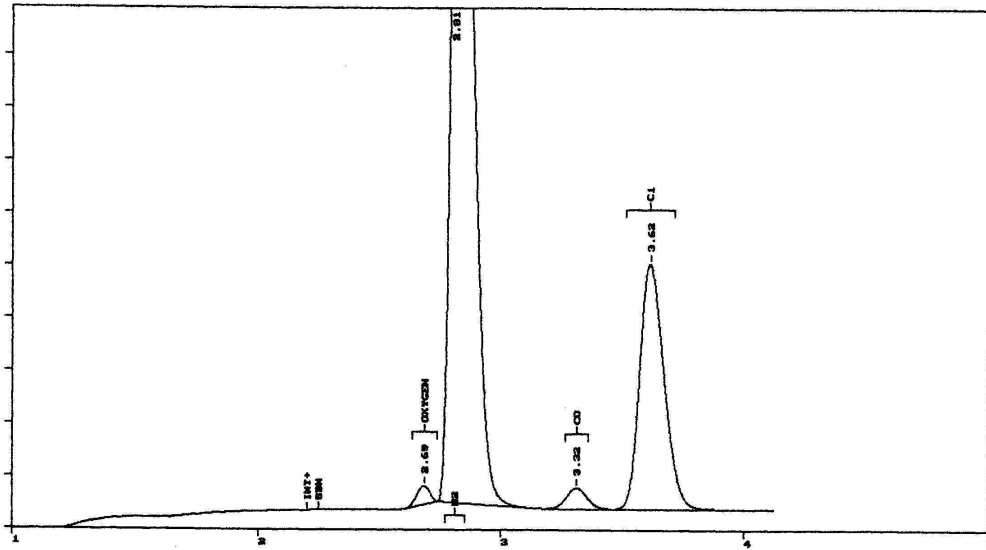


Figure 9. Sample output from the gas chromatograph.

The oil sample that is analyzed in the TVP 95 is gathered in one of two ways. The first way, and the least expensive way, is to purge the top of the cavern and then flow oil into the separator directly from the wellhead. Normally, the first 10,000 barrels of oil removed from the cavern is considered to be roof oil and non-representative of the rest of the cavern. This oil is purged from the cavern before a sample is taken. Sometimes this sampling method is inadequate to obtain a representative sample of cavern oil. An alternate method of gathering an oil sample is to use a downhole sampler constructed by Pencor Laboratories. This sampler is shown in Figure 10. Each downhole sampler has a volume of approximately 10 liters. For the purposes of analysis, four sample tubes provide enough oil to determine the oil vapor pressure. This sampling method has the advantage that the sample may be obtained from greater depths or specific depths within the cavern. This sampling method will more likely produce a representative sample of cavern oil, but at a much greater expense.



Figure 10. Each downhole sampler has a volume of 10 liter. When the downhole sampler supplies the TVP 95, four sample tubes are manifolded together.

3.1 Presentation of Data Obtained with the TVP 95 and the Mini Skid

Since 1993, a great amount of vapor pressure data have been obtained using the separator based analysis tools. These data have been gathered for all caverns and form the bases for our understanding of gas regain. The most recent data referenced in this report are from August 2002. These data are the most important feature of this report. Because of its importance, results for every cavern are presented individually. The vapor pressure is a strong function of the temperature. In order to standardize results, it was decided to gather and present all vapor pressures at 100 °F. Further, regain rates are presented at 100 °F. This graphical presentation of the increase in vapor pressure for each cavern is given in Appendix A.

Because the SPR performance criteria are based upon stream averages, the individual cavern data are aggregated into eight streams. The aggregated regains for the sweet and sour oil from each site are presented below. In order to understand the analysis of regain, it is important to first understand the analysis methods.

Intentionally Left Blank

4.0 Statistical Analysis to Determine the Intrusion Rate for Each Cavern

In order to determine the statistical limits on the gas intrusion rate into each cavern, the bubble-point data are analyzed as follows. It is assumed in this analysis that the gas intrusion rate behaves linearly with time. Another possible model of gas intrusion would be the general oil field depletion model where the rate of intrusion decreases with time and this type of model could just as easily have been applied to the data. However, with the observed scatter in the data, there is not yet definitive evidence that the intrusion rate is decreasing. Consequently, this type of model would be non-conservative. Hence, the linear model is adopted.

$$\Delta bp = a + b(\theta - \theta_{avg}), \quad (1)$$

where Δbp is the change in measured bubble point, θ is the time at which a bubble-point measurement is made, θ_{avg} is the average of all time measurements, and a and b are the linear regression constants obtained from a least squares evaluation. b is also the rate of increase in bubble point with time, which, in this report, is called the gas intrusion rate. With linear least squares, Mickley, Sherwood, and Reed [1957] give the estimate of error variance of the intrusion rate as

$$s_e^2(b) = \frac{s_e^2(\Delta bp)}{\sum (\theta_i - \theta_{avg})^2}, \quad (2)$$

where $s_e^2(b)$ is the variance of the error on the intrusion rate, b , and $s_e^2(\Delta bp)$ is the variance of the individual measurement error associated with the TVP 95. The variance of the TVP 95 has been determined to be approximately 0.62 psi [Hinkebein, 1995]. This value, however, does vary from cavern to cavern.

The value of the standard deviation associated with the measurement of the gas intrusion rates is the square root of the variance,

$$s_e(b) = \sqrt{s_e^2(b)}. \quad (3)$$

Values of the intrusion rates and their standard deviation for each cavern, referenced at 100 °F, are given in Table 1.

The intrusion rates in Table 1 reflect the change in bubble points in oil stored the caverns. Since some of the caverns are only partially full, and oil has been added to some caverns over time, and completely swapped out of other caverns, the changes in bubble points do not necessarily reflect gas intrusion into the caverns. As a result, the values given in Table 1 are illustrative of the actual intrusion rates for each cavern and represent our best estimate of the intrusion rate.

Table 1. Standard Deviation for Individual Cavern Historical Intrusion Rates at 100 °F. (Aug. 2002)

Bayou Choctaw Cavern	Intrusion rate (psia/year)	Standard Deviation for Intrusion Rate (psi/year)	Bryan Mound Cavern	Intrusion rate (psia/year)	Standard Deviation for Intrusion Rate (psi/year)	Big Hill Cavern	Intrusion rate (psia/year)	Standard Deviation for Intrusion Rate (psi/year)	West Hackberry Cavern	Intrusion rate (psia/year)	Standard Deviation for Intrusion Rate (psi/year)
15	0.00	0.07	1	0.28	0.21	101	0.12	0.08	6	0.00	0.06
17	0.35	0.20	2	0.39	0.05	102	0.02	0.07	7	0.00	0.27
18	0.01	0.53	4	0.00	0.05	103	0.42	0.17	8	0.00	0.09
19	0.00	0.05	5	0.00	0.04	104	0.53	0.15	9	0.04	0.09
20	0.00	0.06	101	0.81	0.16	105	0.41	0.13	11	0.00	0.06
101	0.00	0.25	102	0.05	0.04	106	0.34	0.82	101	0.00	0.04
			103	0.97	0.20	107	0.61	0.33	102	0.02	0.19
			104	0.00	0.06	108	0.75	0.51	103	0.51	0.11
			105	0.03	0.08	109	0.29	0.38	104	0.00	0.07
			106	0.03	0.75	110	0.00	0.14	105	0.00	0.05
			107	0.49	0.24	111	0.49	0.29	106	0.00	0.06
			108	0.01	0.04	112	0.17	0.18	107	0.71	0.07
			109	0.22	0.20	113	0.90	0.39	108	0.00	0.06
			110	0.09	0.36	114	0.50	1.69	109	0.00	0.08
			111	1.02	0.35				110	0.00	0.08
			112	2.98	1.84				111	0.09	0.12
			113	0.13	0.06				112	0.00	0.05
			114	0.60	0.06				113	0.38	0.06
			115	0.32	0.41				114	0.00	0.05
			116	0.25	0.10				115	0.00	0.11
									116	0.00	0.10
									117	0.00	0.03

In Table 1, the standard deviations on the intrusion rates are often observed to be large relative to the size of the intrusion rates themselves.

4.1 Aggregation of Individual Cavern Data into Streams

Blending of oil streams allows for less oil to be degassed while still allowing the aggregate stream to meet specifications. Further, this is appropriate because the hydraulic requirements for a max-rate drawdown require all caverns of a stream to be blended using proportional flow. In addition, the uncertainty associated with the blended stream is less than that of the individual caverns. For any given stream, the blended bubble point, bp_m , is

$$bp_m = \sum_i \frac{V_i}{V_t} * bp_i, \quad (4)$$

where V_i and bp_i is the volume and bubble point of cavern i , and V_t is the total volume of the stream. Similarly, the intrusion rate of the aggregate of blended oil, b_m , is given by

$$b_m = \sum_i \frac{V_i}{V_t} * b_i \quad (5)$$

where b_i are the individual cavern intrusion rates. The variance of the intrusion rate for the blended oil stream is (Bowker and Lieberman, [1972])

$$s_e^2(b_m) = \sum_i \left(\frac{V_i}{V_t} \right)^2 s_e^2(b_i) \quad (6)$$

where $s_e^2(b_i)$ is the variance of the intrusion rate for each individual cavern. The impact of Equation (6) is to make the variance for the stream be less than the variance for the individual caverns. The standard deviation of the intrusion rate is

$$s_e(b_m) = \sqrt{s_e^2(b_m)} . \quad (7)$$

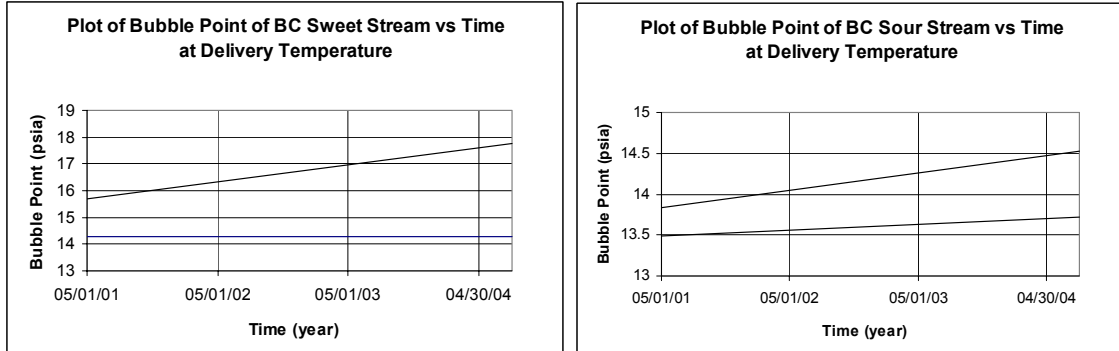
The aggregate intrusion rates and variances for the primary oil streams within the SPR are given at 100 °F in Table 2. In this table, the Big Hill sour stream has the largest average intrusion rate as well as the greatest associated error. Big Hill sweet, Bryan Mound sweet, and Bryan Mound sour, have roughly equivalent intrusion rates of 0.2 – 0.3 psi/year. Gas intrusion at West Hackberry and Bayou Choctaw is significantly less than gas intrusion elsewhere. The error associated with the Big Hill data is observed to be much larger than other errors. From the data, it is not possible to say whether this variation is based on cavern variation or measurement error.

Table 2. Blended Stream Intrusion Rates and Standard Deviation of Average Intrusion Rate at 100 °F (Aug., 2002) (MMB is millions of barrels)

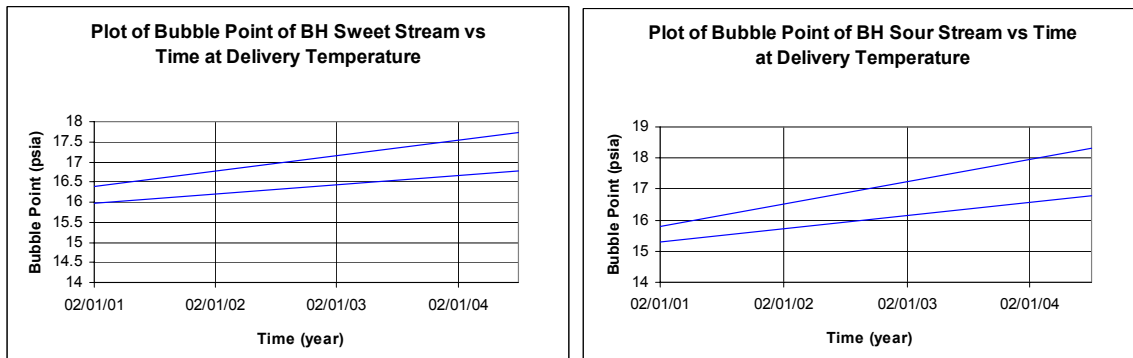
Stream Intrusion Rates	Volume of Stream (MMB)	Stream Average Intrusion Rate (psi/yr)	Standard Deviation of Stream Average Intrusion Rate
BC Sweet	22.14	0.00	0.05
BC Sour	49.15	0.08	0.07
BH Sweet	27.18	0.24	0.08
BH Sour	74.13	0.45	0.15
BM Sweet	69.60	0.21	0.10
BM Sour	151.72	0.29	0.05
WH Sweet	75.83	0.13	0.05
WH Sour	90.15	0.01	0.02

Regain rates are also projected into the future in order to plan for degasification operations. These data are presented in Figures 11 through 18 at design delivery temperatures. It is noted that the design delivery temperature is 90 °F at Bayou Choctaw, Bryan Mound, and West Hackberry, and 95 °F at Big Hill. For this analysis, we have also used the design cooling water temperatures. During very limited periods in the summer, the cooling water may be above these design temperatures. Hence, the predicted vapor pressures may be low in these instances. Two curves are presented for each stream. The lower curve is the average projected bubble point while the upper curve is the average plus two standard deviations of uncertainty. The upper curve has a 95 % probability of bounding the maximum regain in future years. Using the average projected

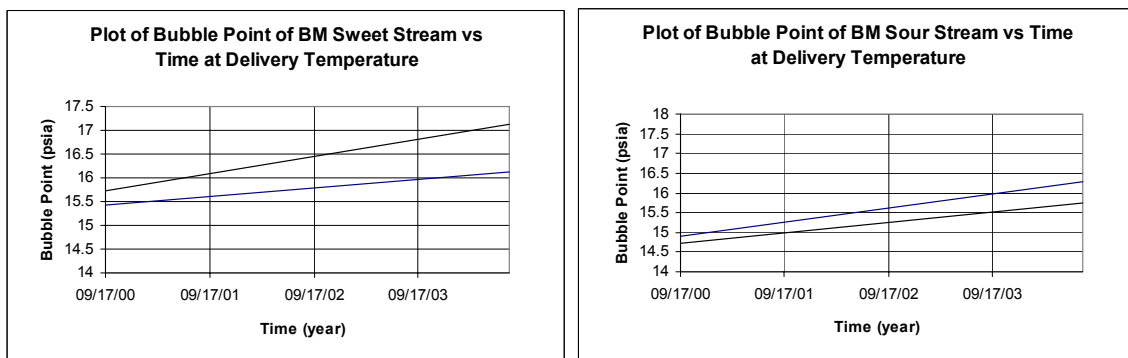
values, all of the aggregate streams in the SPR, except the streams at Bayou Choctaw, will have periods where the delivery criterion of an atmospheric bubble point is exceeded. The right-hand date displayed on these figures is August, 2004. The individual cavern data that support these curves are presented in Appendix A.



Figures 11 and 12. The projected bubble points of the sweet and sour streams at Bayou Choctaw. These curves are presented at delivery temperature of 90° F. The projected bubble points are nominally atmospheric, as determined from historical data. In 2004, the anticipated bubble point for the sour stream will be approximately 13.8 psia while the sweet stream is anticipated to rise to approximately 14.3 psia.

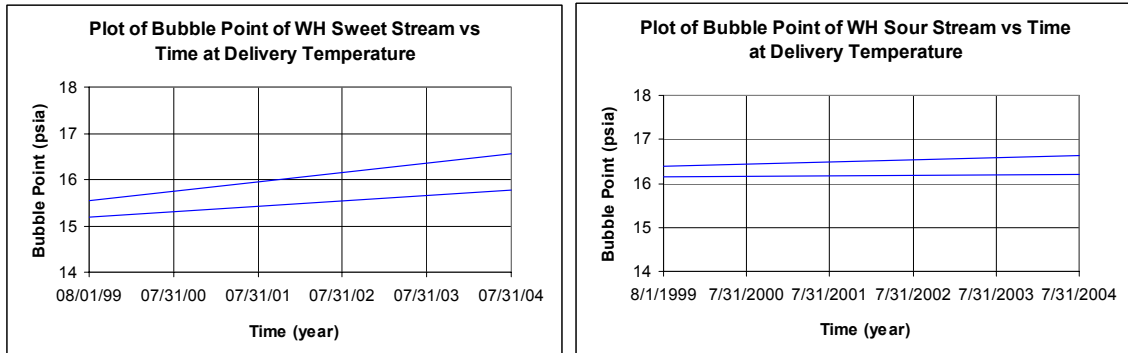


Figures 13 and 14. The projected bubble points of the sweet and sour streams at Big Hill. These curves are presented at delivery temperature of 95° F. In 2004, the anticipated bubble point for both the sweet and sour stream will be approximately 16.6 psia.



Figures 15 and 16. The projected bubble points of the sweet and sour streams at Bryan Mound. These curves are presented at delivery temperature of 90 ° F. In 2004, the

anticipated bubble points for the sweet stream is 16.2 while that for the sour stream is approximately 15.7 psi.



Figures 17 and 18. The projected bubble points of the sweet and sour streams at West Hackberry. The delivery temperature at West Hackberry is 90 ° F. The sour stream has a smaller error than the sweet stream. In 2004, the sweet stream is projected to rise to 15.7 psia while the sour stream has very little regain and is 16.3 psia.

Intensionally Left Blank

5.0 The Compositional Analysis Methods of the TVP 95

We will now examine the consequences of gas releases. As stored oil absorbs intruding gas, its vapor pressure increases. With movement of this oil to storage tanks, gases may be liberated. Some of these gases (methane, ethane, carbon dioxide, and nitrogen) have no regulatory consequences. However, other released gases, such as the propane plus fraction are regulated. Further, some of the gases, such as H₂S, and benzene, have more serious health effects. Consequently, it is important to obtain a compositional analysis of the light ends of crude oil.

Toward this end, the goal of the compositional analysis is to determine the composition of the oil, as it is stored in the cavern. In order to determine the composition of the cavern oil, it has been necessary to determine the composition of the off gas because liquid gas chromatographs have not yet been proven to be field devices. Testing is currently underway to determine if newly-available instruments may be able to provide a direct measurement. In order to arrive at the relationships between the gas phase compositions, y_i , and the feed liquid phase compositions, z_i , a mass balance on the TVP-95 separator yields Equation (8),

$$Fz_i = Gy_i + Lx_i, \quad (8)$$

where F is the molar feed rate, L is the oil flow rate, and G is the gas production rate. In addition to the mass balance relationship, the chemical equilibrium between the liquid and the gas phases is given by

$$K_i = \frac{y_i}{x_i}, \quad (9)$$

where K_i is the equilibrium ratio or K factor.

Solving for the feed composition, z_i , and eliminating the oil flow rate yields Equation (10).

$$z_i = \left(\frac{G}{F}\right)y_i + \left(1 - \frac{G}{F}\right)\frac{y_i}{K_i}. \quad (10)$$

Gathering terms yields an expression for the feed composition in terms of the gas composition,

$$z_i = y_i \left(\frac{\left(1 - \frac{G}{F}\right)}{K_i} + \frac{G}{F} \right). \quad (11)$$

A similar equation may be generated for each component up through hexane. The C_7^+ composition is determined as shown in the Equation (12). These equations allow the feed composition for the light ends to be determined.

$$z_{C_7^+} = 1 - \sum_{i=1}^{N-1} z_i \quad (12)$$

In the operation of the TVP 95, we obtain measurements of the total gas flow, G , as well as the separator liquid, L . Chromatographic measurements of the off gases released yield the mole fraction measurements of the light end gas components.

The K factors in the above equations are determined by using the SRK equation of state. The algorithm to compute the K -factors is described in detail by Reid, Prausnitz, and Poling [1987], Example 8-14. One of the features of this solution algorithm is the specification of binary interaction coefficients. For the calculations presented in this report, these interaction coefficients have all been set to zero to allow for the greatest compatibility with standard process simulators.

Equations (11) and (12) may be used with chromatographic data obtained from the off gas released from the separator. These analyses allow the light end compositions to be determined. The recombined liquid compositions, expressed as mole fractions, for all caverns are presented in Appendix B.

6.0 Plume Analyses of Gaseous Emissions Using the Industrial Source Complex-Short Term (ISCST) Gaussian Dispersion Model

The ISCST (Industrial Source Complex Short Term) model (ISCST3, Version 4.5i, USEPA [2000]) is the currently accepted air model for both Texas and Louisiana and is developed and approved by the EPA. This model simulates a steady-state Gaussian plume. A Gaussian plume is characterized by having a normal distribution of concentration perpendicular to the flow, as shown in Figure 19.

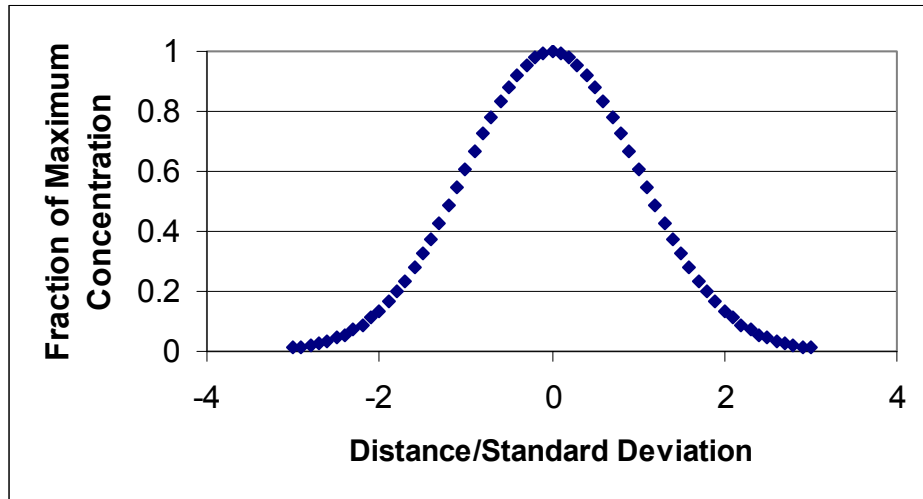


Figure 19. Gaussian concentration distribution transverse to flow.

A full-scale drawdown will result in the transfer of gassy oil to oil-storage tanks. At the tanks, gas will evolve from the oil and disperse in the air. These gaseous emissions contain components that are regulated by environmental and health regulations. Both quantity and concentration limits must be met when oil is delivered to tanks. The quantity of gas evolved is determined from the gas-oil ratio at the temperature and pressure of the oil in the storage tank. The total gas released is the gas-oil ratio times the total amount of oil moved. It has been observed that tank residence time has almost no effect on the amount of gas released.

The compositional data obtained in Section 5.0 is used in combination with the total quantity of evolved gas to determine the quantity of controlled gases released during an oil transfer. It is these controlled gases that must be limited during drawdown.

The total quantity of evolved gases can be limited by controlling oil flow rates and gas-oil ratios. Calculations have been performed to determine the maximum oil flow rates for specified maximum plume concentrations of H_2S , benzene, and total hydrocarbons.

These computations represent our effort to model the dispersion phenomena using methods approved by the state regulatory agencies. The answers obtained from this study may be used to provide an estimate of the maximum oil flow rates. There are, however, a number of limitations to this modeling exercise that must be considered so that we develop an appropriate level of confidence in the final answers. Gaussian dispersion modeling is calibrated to give adequate accuracy in the far field. This type of model is

not known for its accuracy near the source. Hence, the environmental conditions near the tanks must be monitored to assure that observed concentrations remain within allowed limits.

Further studies are currently underway to address the weaknesses in the Gaussian modeling approach. These studies are using a computational fluid dynamics (CFD) code, FLUENT, to examine the near field effects. These studies will be completed in the coming year.

6.1 Single Tank Modeling - Assumptions and Approximations and Modeling Basis

In order to obtain a better agreement between calculated air emissions concentrations and observed conditions, several Sandians (Einfeld [1993] and Hinkebein [1994]) have run the ISCST Gaussian dispersion code. The purpose of these analyses was to adjust the ISCST model with observed field conditions so that subsequent modeling is more realistic.

In 1993, very gassy oil from Bryan Mound Caverns 101, 103, 108, 109, and 112 was pumped into Tank #1 (diameter 222 ft and height 32 ft) at a rate of 25 MBH (25,000 barrels per hour) (DynMcDermott [1993]). For all SPR emissions, it is assumed that the H₂S concentration is nominally 2% of the vapor phase and the benzene concentrations were 0.1% of the vapor phase. For this test, the concentration of H₂S in the vapor phase for this test was also approximately 2%. When this vapor evolved, it mixed with air in the dead space above the floating roof. The maximum concentration of H₂S, measured at the main vents, was 3500 ppm. Concentrations of 20 ppm were observed at the base of the tank. These concentrations occurred for a flow rate of 25 MBH and a GOR of 6.5 SCF/BBL. Because of the high concentration at the top of the tank, any atmospheric condition that allows this gas to fall to the ground without being diluted could lead to a potentially hazardous condition. This type of dense gas behavior is typically observed at low wind conditions.

Initial modeling with the ISCST code was performed with a single tank and wind stability condition, E, where E is a variable used in the ISCST code to denote very stable wind conditions. This condition provides for a very coherent plume and higher airborne concentrations. This wind stability condition is also conservative because stable wind leads to higher and less dispersed concentrations in air. These calculations, however, produced air concentrations far less than was observed in the Bryan Mound tank test. To compensate for this underprediction of airborne concentration, the *tank height* was varied to obtain a match to experimental conditions. This artificial variation in tank height was performed because some phenomena are taking place that the ISCST code does not model accurately. These phenomena include tank-induced changes in wind direction (wake effects), minor density differences between the evolving gas and the surrounding air, and local topography variations. Hence, the height of the tank was varied to compensate in part for these effects. It is further known that the ISCST model is not accurate near the tank where local turbulence effects and density driven flows occur. The far field analysis (observed from the data to be distances greater than 400 m) is much

more accurate and the effect of modifying the tank height is very small, within 10% at 400 m plus distances.

Further, the actual source term for these calculations is an *area source*. In order to simulate the area source, the tank was subdivided into 16 equal areas. Each of these areas was approximated by a point source. This technique provides for an areal distribution of the gases and numerical results that match the Bryan Mound tank test observations within 25%.

For the modeling of conditions different from those of the tank test, it is assumed that the tank height remains at one meter. This assumption is believed to be conservative. Further, it is assumed that the *wind stability* condition is E, i.e., very stable, for all projected operating conditions. This assumption provides for a very coherent plume and also higher airborne concentrations. This wind stability assumption is conservative because more stable wind conditions lead to higher and less dispersed concentrations in air.

6.2 Single Tank Model Results

The ISCST model was used to determine the concentrations of H₂S, benzene, and total hydrocarbons. A typical result that provides a good data fit to the Bryan Mound tank test is the H₂S plume shown in Figure 20. This plume was calculated to match field conditions for a total gas release of 100 MSCF/hr, 2% H₂S, and a wind speed of 3 meter/sec. The source of gas for this calculation is 100 MSCF/hr: This is the product of the oil flow rate in MBD and the gas-oil ratio expressed in SCF/BBL. An important feature of the model is that the vapor concentration in the plume is directly proportional to the molar gas release rate and inversely proportional to the wind speed:

$$\text{Concentration in plume} = \frac{(\text{Constant})(\text{Oil flow rate})(\text{Gas-Oil Ratio})(\text{Vapor mole fraction in emitted gases})}{(\text{Wind Speed})} \quad (13)$$

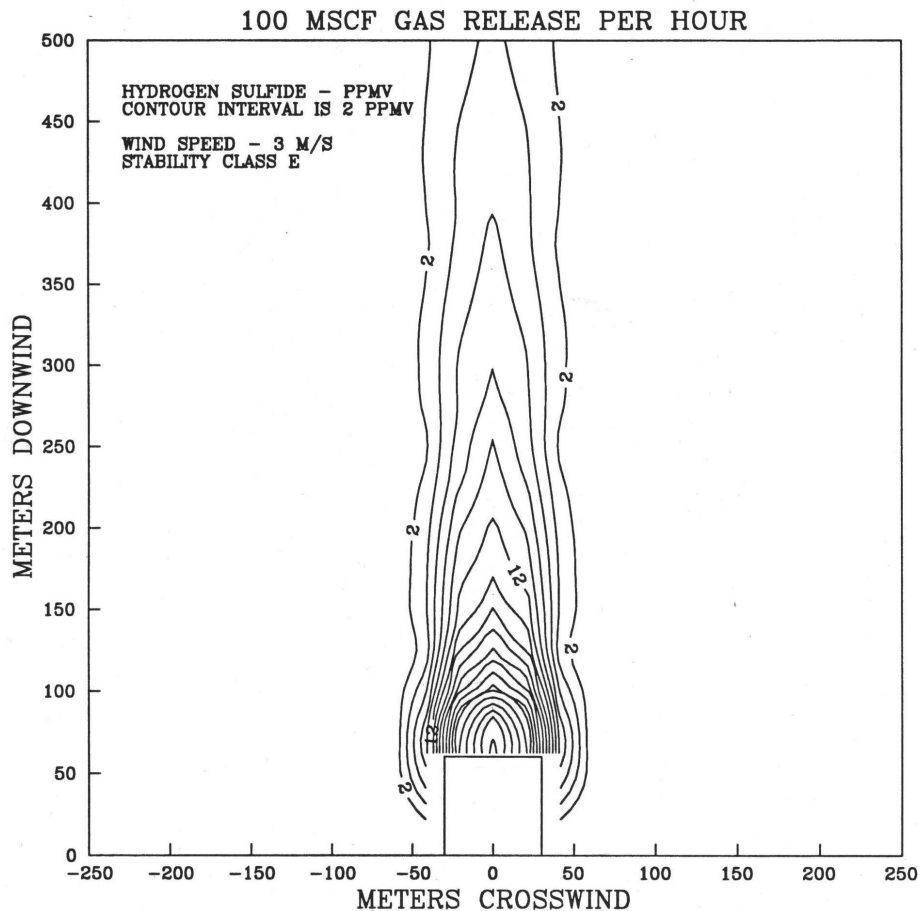


Figure 20. Plots of H₂S concentration in a 100 MSCF/hr plume.

Equation (13) together with Figure 20 may be used to estimate the concentration of any component at any conditions of wind speed, GOR, oil flow rate, or vapor mole fraction. Stated another way, Figure 20 may be used to generate complete concentration profiles for all possible oil flow rates, GORs, wind speeds, and species mole fraction conditions.

A wind speed distribution for Port Arthur, TX in 1992 is presented in Figure 21. From this figure, wind speeds less than 3 meters/sec (7 MPH) occur approximately 30 % of the time. The wind speed that is selected will strongly influence the oil delivery rate and the probability of being able to deliver. For a given GOR, vapor mole fraction, and target concentration in the plume, by Equation (12), the oil flow rate is directly proportional to the wind speed. From a safety point of view, the SPR desires to have 95% reliability that the maximum actual concentration will be less than a target concentration. In Figure 21, the wind speed will be greater than 1 meter/sec (2.2 MPH) 95% of the time. At higher wind speeds, the model predicts that the concentrations will be lower. The GOR and the oil flow rate will be determined to meet this criterion.

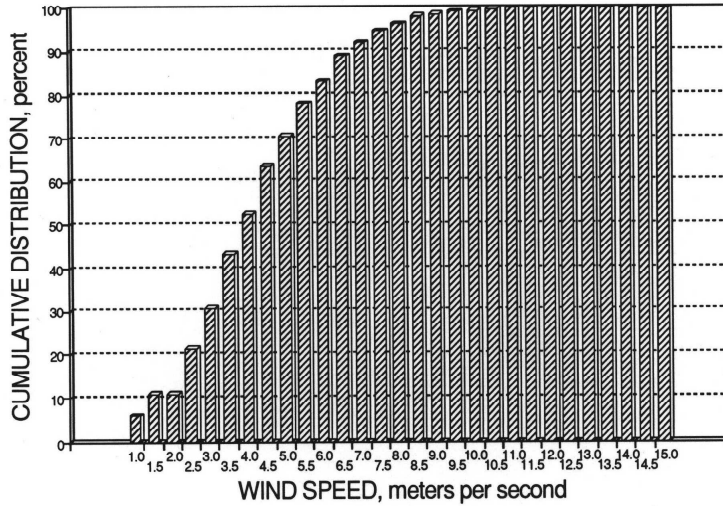


Figure 21. Cumulative distribution of wind speed for Port Arthur in 1992.

6.3 Deliverability Based upon H₂S and Benzene Concentration

The most critical toxic component of oil is H₂S. Its maximum concentration is regulated by a number of codes. OSHA (29CFR1910.1000) has recommended worker safety limits of 10 ppm. Both Texas and Louisiana impose limits of exposure for non-workers. 30TAC112.31 limits the concentration of H₂S to 0.08 ppm where the plume may fall on residential property. A similar regulation, 30TAC112.32, limits the concentration of H₂S to 0.12 ppm where the plume may fall on other than residential property.

If we examine oil deliverability for a typical storage tank condition, we find that the maximum concentration of the plume may fall approximately 50 feet from the tank edge. Because of the proximity of some of our tanks to the property line, there are times when the maximum concentration will be beyond our fence line (in some cases this is 50 ft). If we consider a scenario where we pump oil at 30 MBH (0.72 MMB/day), then the resultant deliverability is given in Figure 22.

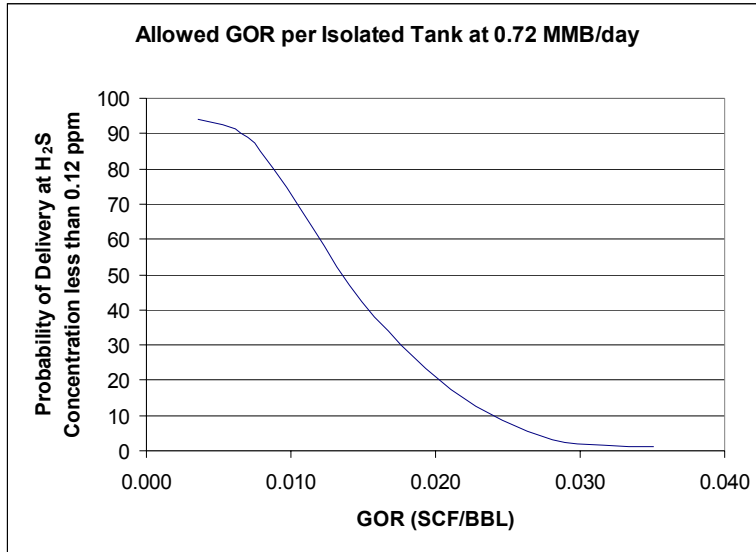


Figure 22. Emissions of H₂S for deliverability of oil at 30 MBH. A GOR of 0.004 SCF/BBL will produce a maximum plume concentration of less than 0.12 ppm for 95% of the time. The vapor concentration of H₂S is assumed to be 2% at the source and the maximum concentration in Figure 20 is 38 ppm.

If the GOR exceeds 0.004 SCF/BBL, the maximum plume concentration for H₂S will exceed 0.12 ppm. Hence, this criterion is interpreted that the GOR must be less than 0.004 SCF/BBL in order for the oil to be deliverable. This GOR criterion is so small as to be essentially zero. In order to improve oil deliverability, the SPR has decided to implement H₂S scavenging during full max rate drawdown..

If H₂S is scavenged, then the next most critical component of the oil is benzene. A curve similar to the above has been generated for benzene, as shown in Figure 23. From this figure, the GOR criterion of 0.6 SCF/BBL is required to keep the benzene concentration below 1.0 ppm, (OSHA 29CFR1910.1028).

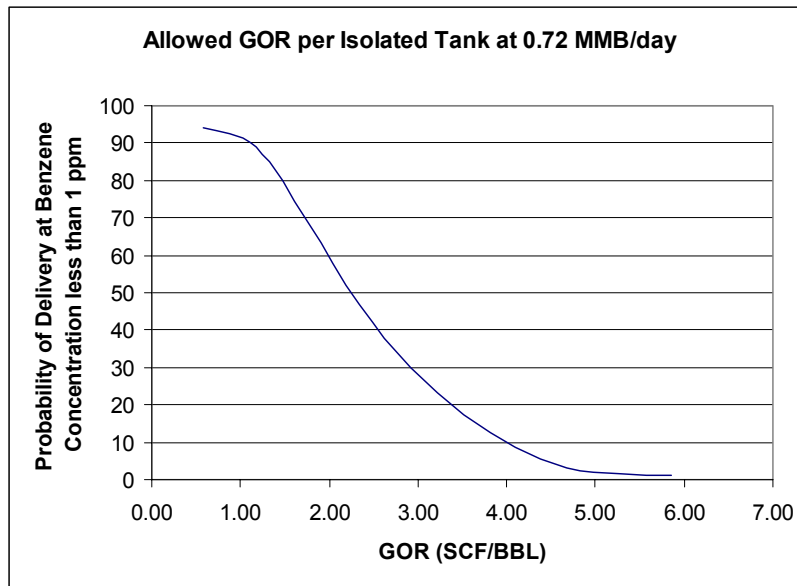


Figure 23. Emissions of benzene for deliverability of oil at 30 MBH. A GOR of 0.6 SCF/BBL will produce a maximum benzene plume concentration of 1.0 ppm for 95 % of the time.

6.4 Discussion of Plume Modeling

As has been mentioned before, these computations represent our efforts to model the dispersion phenomena from a single tank in accordance with state environmental regulations. Some of the limitations to this modeling exercise have already been considered. The Gaussian dispersion model, ISCST, tends to predict a lower air concentration of H₂S, benzene, and total hydrocarbons than is actually observed near the tank. In this analysis, we have compensated for the underprediction by artificially lowering the tank height to boost the gas concentration. This compensation produces results that we believe provide a reasonably accurate estimate of what will actually occur around a single tank.

In addition to the already discussed assumptions, some additional considerations cast further uncertainties on the presented results. These additional effects include wake effects, density driven flows, and multi-tank interactions. The potential influence of these effects can be profound because the concentration of hydrocarbons at the top of the tank is so much greater than the concentration near the base of the tank. Hence, it is important to recognize that temporary changes in air conditions can have large, if transient, changes in the gas concentration. As a consequence, we believe that greater accuracy and understanding are needed. The best course would be to devise an experimental and computational program to address these phenomena with a more comprehensive approach. At present, the program is investigating a computational fluid dynamics program to further refine these computations, with special interest in the near field (less than 400m) solutions.

The computational fluid dynamics code, FLUENT, is currently be used to examine the emissions in the vicinity of floating roof storage tanks. This modeling effort was undertaken to resolve some of the near field discrepancies found with the experimental results and the ISCST code. The main problem is that the ISCST results greatly underestimate the near field concentrations. The CFD approach is primarily being used to assure worker safety in the near field as where discrepancies do occur. This modeling effort is using wind tunnel testing and results to check results and to aid with the more accurate prediction of results under actual operating conditions. These results will be completed in 2003.

7.0 Analysis of GOR Regain for Individual Caverns and Combined Streams

In this section, we examine the effect of regain on gas-oil ratio. In Section 4.0 on vapor pressure regain, it was seen that the inventory in some caverns will have vapor pressures greater than one atmosphere at delivery temperature. If gassy oil is transferred to storage tanks, emissions will be produced and have the consequences modeled in the plume analysis section. In that section, it was observed that almost no off gas is allowed in meeting the H₂S standard. If H₂S is scavenged, however, up to 0.6 SCF/BBL of gas may be released within the benzene standard (for 30 MBH delivery rates).

The gas-oil ratio for SPR oil is not frequently a directly measured quantity. Rather the usual measurement scheme involves the determination of the bubble-point pressure. By using the compositional data as well as the bubble-point pressure, the gas-oil ratio can be calculated with the SRK equation of state. This calculated GOR quantity is less accurate than the directly measured bubble point.

As was the case when the recombined compositions of the oil phase were determined, the computational procedures outlined in Reid, Prausnitz, and Poling [1987] were used. Please refer to Example 8-14. The current best value for the GOR, its rate of increase, and the uncertainty associated with the measurements is given in Table 3 for the standard measurement conditions of 100°F.

From Table 3, the variability in GOR increase rate is apparent. Based on the current data, the GOR increase rates at Bayou Choctaw and West Hackberry are very low. At Big Hill and Bryan Mound increase rates are in some cases large but variable from cavern to cavern. A few caverns, with the largest intrusion rates, (BM112, BH114) are currently not being used for significant oil storage. After the SPR completes construction of a degassification facility, these caverns may be used for additional storage. Further, the data used to generate Table 3 can be used to determine the optimal sequencing for degassification. In Table 4, the stream averages are presented.

Table 3. Cavern gas-oil ratios, GOR increase rates, and measurement uncertainty as analyzed at 100 °F. When the bubble point is less than atmospheric, the calculated GOR is negative. This negative value implies a GOR deficit. In reality, no gas is evolved. These data represent information available as of August 2002.

Bayou Choctaw Cavern	GOR (SCF/BBL)	GOR Increase Rate (SCF/BBL/year)	Standard Deviation for Increase Rate (SCF/BBL/year)	Bryan Mound Cavern	GOR (SCF/BBL)	GOR Increase Rate (SCF/BBL/year)	Standard Deviation for Increase Rate (SCF/BBL/year)
15	-0.05	0.00	0.04	1	-0.55	0.00	0.07
17	-0.27	0.07	0.14	2	0.50	0.16	0.11
18	0.26	0.02	0.30	4	2.73	0.07	0.10
19	0.30	0.00	0.04	5	1.73	0.00	0.02
20	2.23	0.01	0.04	101	-1.31	0.06	0.11
101	0.04	0.00	0.08	102	1.50	0.02	0.04
				103	0.48	0.30	0.10
				104	5.76	0.18	0.11
				105	1.68	0.01	0.03
				106	0.91	0.98	0.29
				107	-2.44	0.00	0.27
				108	4.77	0.08	0.06
				109	-0.57	0.00	0.03
				110	-0.84	0.00	0.11
				111	3.20	0.75	0.11
				112	5.44	6.04	4.79
				113	-0.85	0.00	0.05
				114	1.10	0.31	0.04
				115	3.78	0.32	0.30
				116	4.18	0.00	1.23
Big Hill Cavern	GOR (SCF/BBL)	GOR Increase Rate (SCF/BBL/year)	Standard Deviation for Increase Rate (SCF/BBL/year)	West Hackberry Cavern	GOR (SCF/BBL)	GOR Increase Rate (SCF/BBL/year)	Standard Deviation for Increase Rate (SCF/BBL/year)
101	3.96	0.23	0.07	6	0.92	0.00	0.03
102	1.26	0.01	0.04	7	1.41	0.00	0.61
103	4.98	0.34	0.11	8	0.43	0.00	0.08
104	3.82	0.27	0.09	9	1.53	0.00	0.04
105	-0.76	0.00	0.04	11	0.89	0.00	0.03
106	-0.31	0.00	0.38	101	1.48	0.00	0.02
107	-0.08	0.13	0.03	102	1.37	0.00	0.05
108	1.11	0.25	0.13	103	-0.16	0.10	0.04
109	-0.63	0.00	0.10	104	0.55	0.00	0.04
110	1.31	0.00	0.08	105	1.71	0.00	0.02
111	0.90	0.13	0.07	106	0.83	0.00	0.04
112	0.85	0.10	0.05	107	0.15	0.20	0.03
113	0.67	0.22	0.10	108	1.86	0.00	0.05
114	2.82	0.00	0.54	109	0.86	0.00	0.05
				110	1.27	0.00	0.04
				111	1.20	0.00	0.05
				112	1.12	0.00	0.03
				113	-0.54	0.03	0.04
				114	1.05	0.00	0.03
				115	1.67	0.00	0.06
				116	1.56	0.00	0.07
				117	1.47	0.00	0.02

Table 4. Projected stream averages of the GOR, its increase rate, and statistics at 100°F (Aug, 2002).

Stream Intrusion Rates	Volume of Stream (MMB)	Stream Average GOR (SCF/BBL)	Stream Average GOR Increase Rate	Standard Deviation of Stream Average Increase Rate
BCSweet	22.14	0.93	0.02	0.22
BCSour	49.15	0.00	0.02	0.04
BH Sweet	27.18	1.33	0.07	0.03
BH Sour	74.13	0.47	0.10	0.06
BM Sweet	69.60	2.15	0.16	0.19
BM Sour	151.72	1.36	0.12	0.03
WH Sweet	75.83	1.01	0.03	0.10
WH Sour	90.15	1.08	0.00	0.01

In Figures 24-31, the stream average GOR data are presented at delivery conditions. For Bayou Choctaw and West Hackberry, the average GOR increase remains below 0.6 SCF/BBL. The remaining streams, at Big Hill and Bryan Mound, have average gas-oil ratios that are now or will grow to greater than 0.6 SCF/BBL.

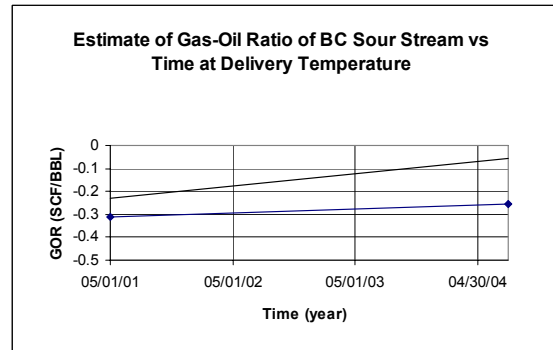
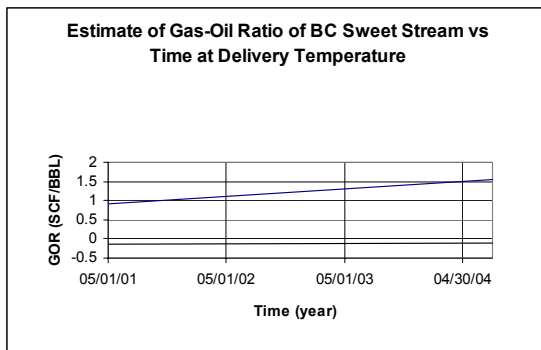


Figure 24 and 25. Projected GOR rate increase brackets showing average increase rate and + 2σ for Bayou Choctaw at the delivery temperature of 90°F.

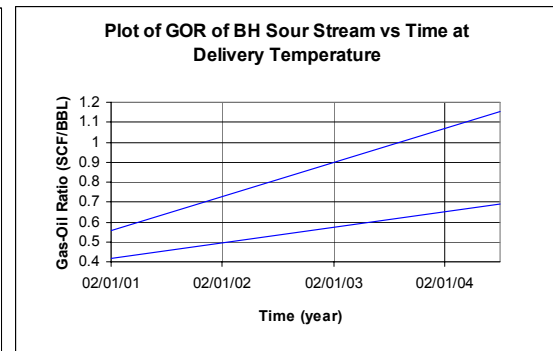
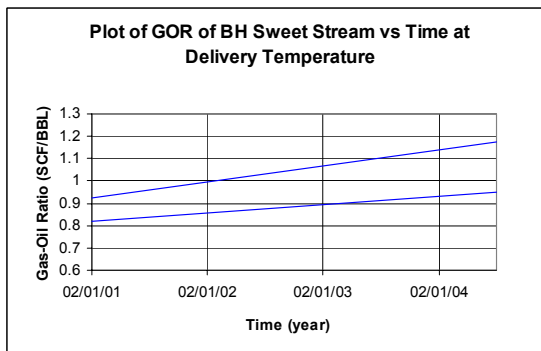


Figure 26 and 27. Projected GOR rate increase brackets showing average increase rate and + 2σ for Big Hill at the delivery temperature of 95°F.

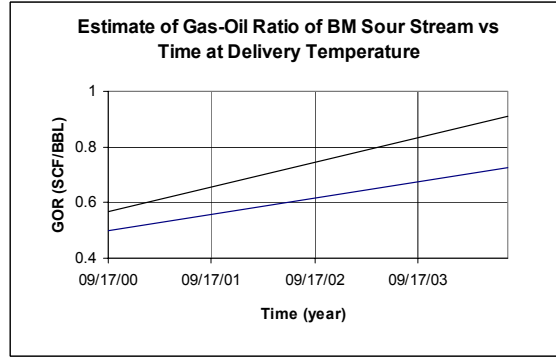
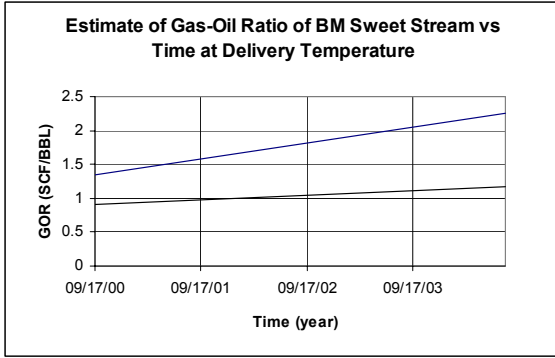


Figure 28 and 29. Projected GOR rate increase brackets showing average increase rate and + 2σ for Bryan Mound at the delivery temperature of 90°F.

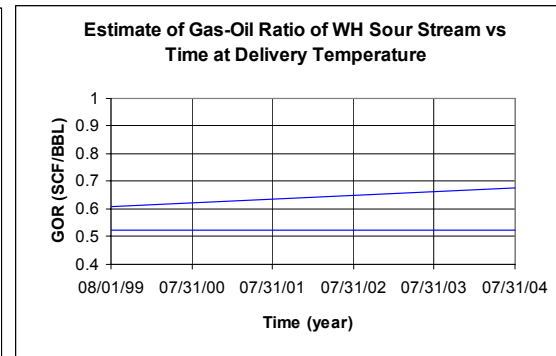
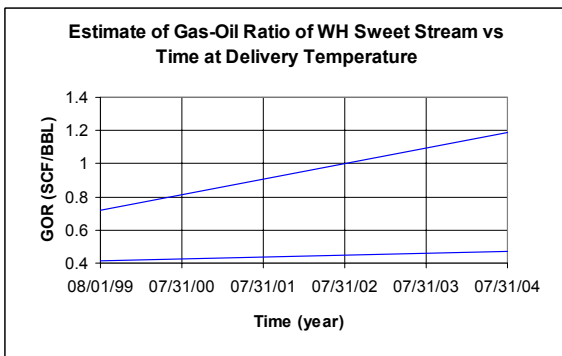


Figure 30 and 31. Projected GOR rate increase brackets showing average increase rate and + 2σ for West Hackberry at the delivery temperature of 90°F.

A comparisons between the bubble point pressure data and the gas-oil ratio data is made in Figure 32 for all data at 100 °F.

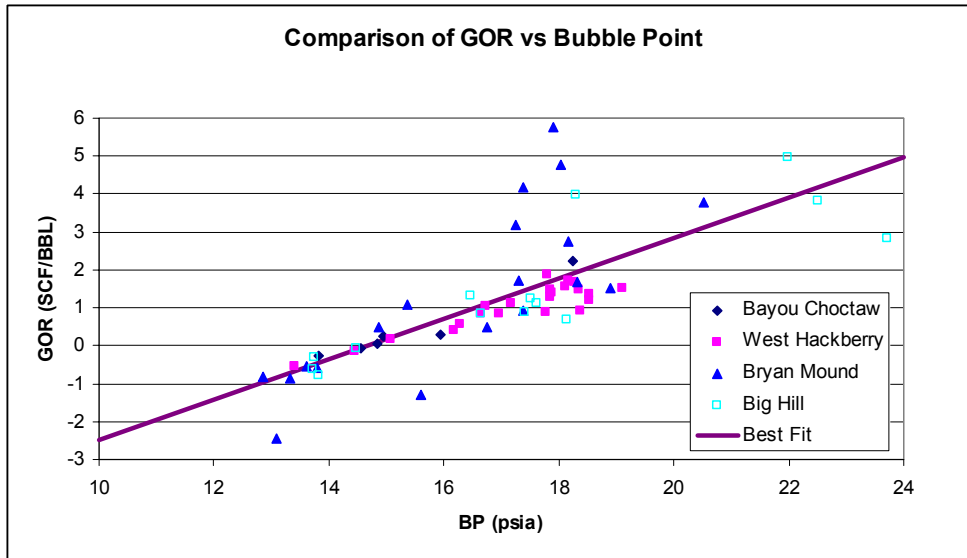


Figure 32. A comparison between the gas-oil ratio and the bubble point pressure for all vapor pressure data. The correlation is $GOR (SCF/BBL) = 0.53 * (BP - 14.7 \text{ psia})$.

The comparison made in Figure 32 points has been analyzed for error. The error associated with this correlation between the gas-oil ratio and the bubble point for all caverns is approximately 1 SCF/BBL for each measurement. It is only with repeated measurements that cavern estimates of error may be reduced.

Intentionally Left Blank

8.0 Conclusions

There are several potential mechanisms of gas intrusion. Gas is observed to enter a cavern suddenly in response to freshwater leaching of a cavern, and it is observed to enter the cavern gradually, perhaps by a permeability mechanism. During the initial leaching of the cavern, most of the intruding gas is swept out of the cavern with the disposed brine. After a cavern is filled with oil, however, small gaseous releases are predominantly captured in the oil phase. During the more normal periods of operation when no fluid is moving, it appears that gas intrusion continues by a permeability mechanism. Because of the inconsistency associated with a generalized permeability model, it is surmised that the gas intrusion either occurs along discrete permeable zones or in response to a permeability enhancement mechanism such as the effect of a disturbed rock zone.

While there is not a present a clear picture of the gas intrusion mechanism, the SPR has at present concentrated its effort on mitigating the readily measured vapor pressure increase. In the future, coming to an understanding of the cause of the increase could have a profound value to the project. It could allow for a rational selection mechanism for new caverns and domes. For this reason, some continued effort should be devoted to this goal.

Measurement of the bubble-point pressure with the TVP 95/mini skid is an effective way of determining gas intrusion. This device provides consistent measurements which are nonbiased and amenable to determination of the oil composition. The normal procedure of closing the vapor phase valve and waiting for steady-state accurately produces the bubble-point pressure. Samples of the vapor phase are then used to compute the feed oil composition. The use of the SRK equation of state with this data gives reproducible compositions for the oil.

When the compositions were examined, it was observed that sour oil has the expected higher concentration of H₂S. Further, the propane concentration of sour oil was approximately 2 % while the propane concentration of sweet oil was approximately 3%. It was also observed that for the same bubble point, sweet oil has a higher GOR than sour oil.

Statistically, the accuracy of all of the streams bubble point pressures was good. The standard deviation associated with these measurements was less than or equal to 0.1 psia for all streams except Big Hill sour. Big Hill sour had a standard deviation of 0.15 psi/year and an average intrusion rate of 0.45 psi/year.

Intrusion rates at Bryan Mound were about 0.2 – 0.3 psi/yr. At Big Hill, the sour stream had an intrusion rate of 0.45 psi/yr, and the sweet stream intrusion rate was 0.2 psi/yr. At the other sites, the intrusion rates were normally 0.1psi/yr or less. Similar results were observed with GOR growth.

Atmospheric dispersion modeling around storage tanks was also performed. The ISCST Gaussian dispersion code was calibrated with the Bryan Mound tank test results of 1993.

This code was then used to determine the maximum GOR that could be delivered to storage tanks under process conditions. H₂S was the most limiting specie and it was found that delivery standards would be violated for GORs in excess of 0.004 SCF/BBL. This extremely small value of allowed H₂S reinforced the need for H₂S scavenging. The second most critical emission specie was benzene. It was found that the maximum GOR was approximately 0.6 SCF/BBL in order to comply with atmospheric regulations for benzene. CFD modeling of the emissions in the near field is currently on going and will provide a greater understanding of the safety implication of releases.

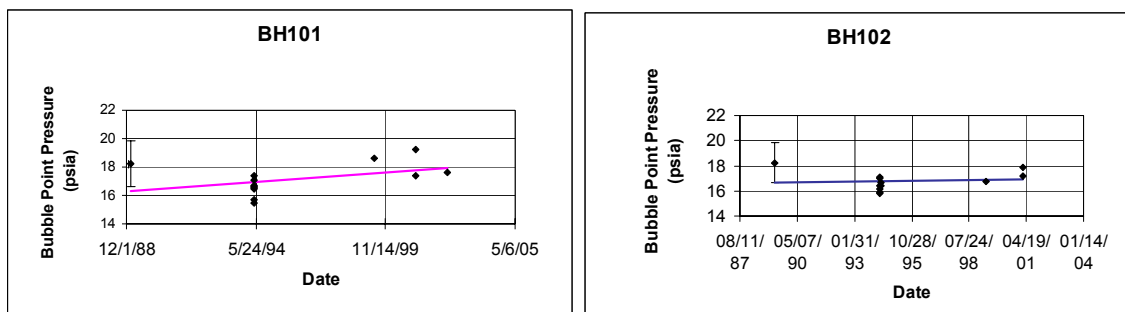
Appendix A. Vapor Pressure History at 100 °F of Individual Caverns in the SPR through Aug., 2002.

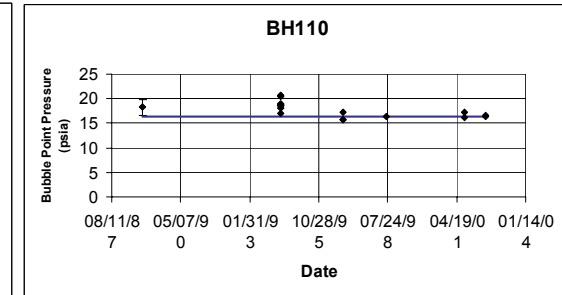
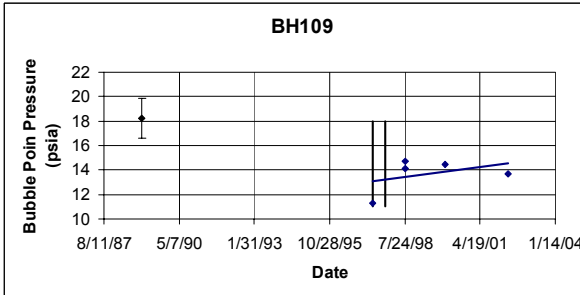
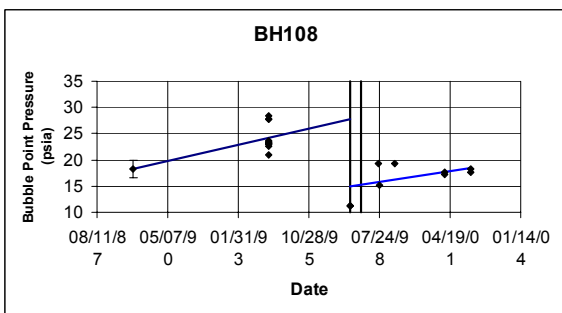
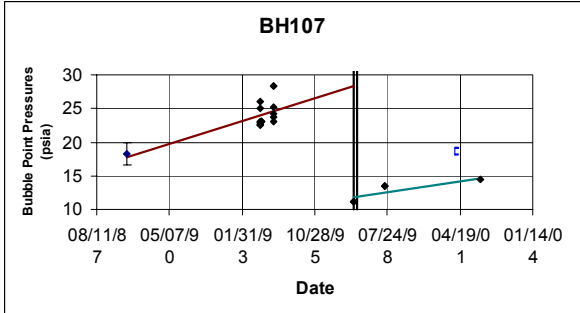
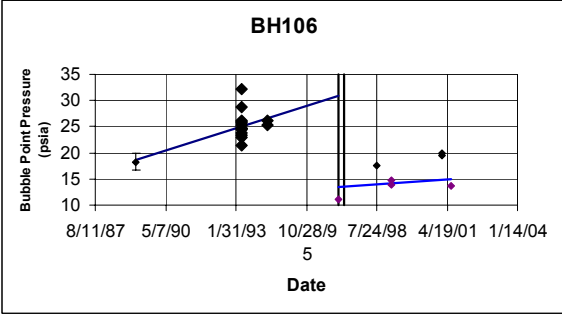
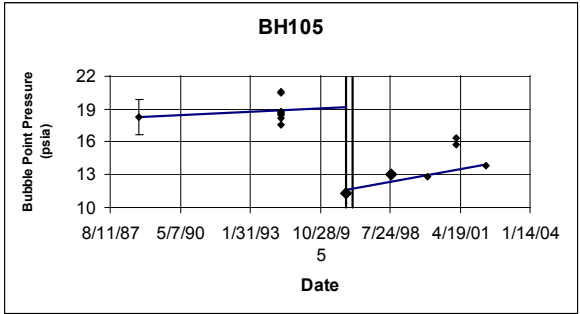
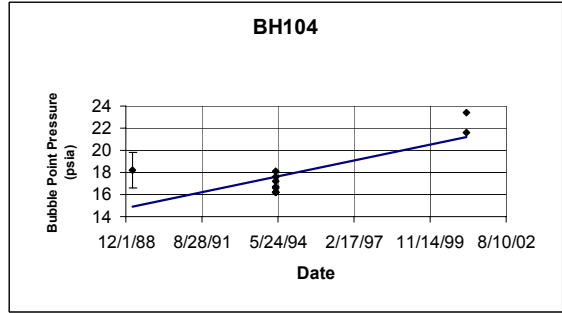
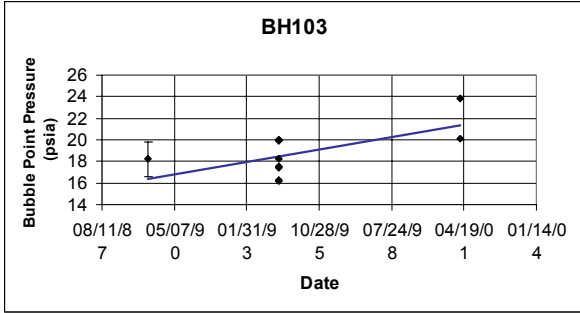
The data showing the vapor pressure history of every cavern within the SPR are presented at 100 °F in this appendix. Individual data points gathered before 1995 were obtained by using the mini skid. Subsequent to 1995, the TVP 95 was used to obtain data. No data exists for the time of cavern fill which typically occurred before 1993-94. Rather, the data were gathered for receipt oil after measurement standards were established. These data were used to establish a representative range for the initial oil in each cavern. Because of the uncertainty of the initial oil vapor pressure, the vapor pressure increase (regain) for caverns with only one set of data are less reliable than for those caverns with multiple data sets.

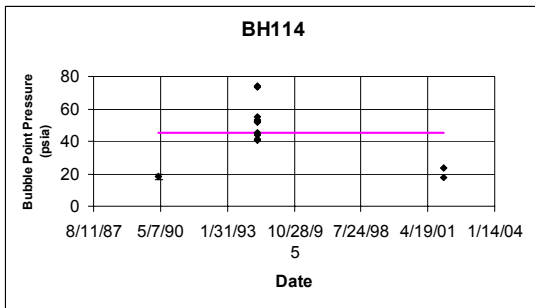
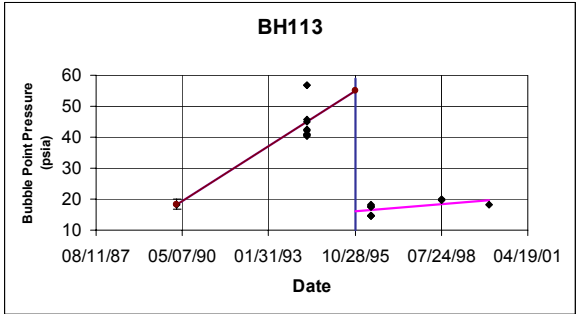
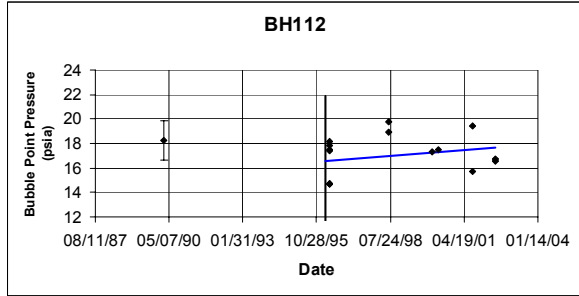
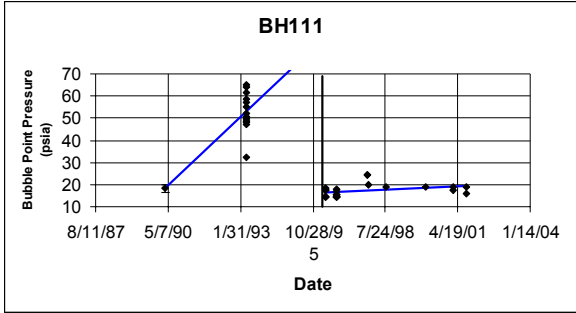
Vertical lines on any plot indicate a complete change in oil vapor pressure, e.g., as would happen after the degasification of the oil stored in the cavern. The first data points after degas were obtained with the TVP 1000. This instrument is not as accurate as the TVP 95, and it may be responsible for further inaccuracy in regain rates after degas.

In some caverns, data points are not included in the least squares regression to determine intrusion rates. Data points for which this occurred are ones that have shown anomalously high concentrations of dissolved nitrogen. These data points were flagged at the time they were gathered, and the caverns were selected for an early resampling. Cavern sampling was performed with a down hole sampler to minimize the effects of cavern integrity testing which tends to add nitrogen to the oil near the cavern roof. If these latter resampled data prove that the earlier data were compromised, then they are presented for completeness but not included in the regression.

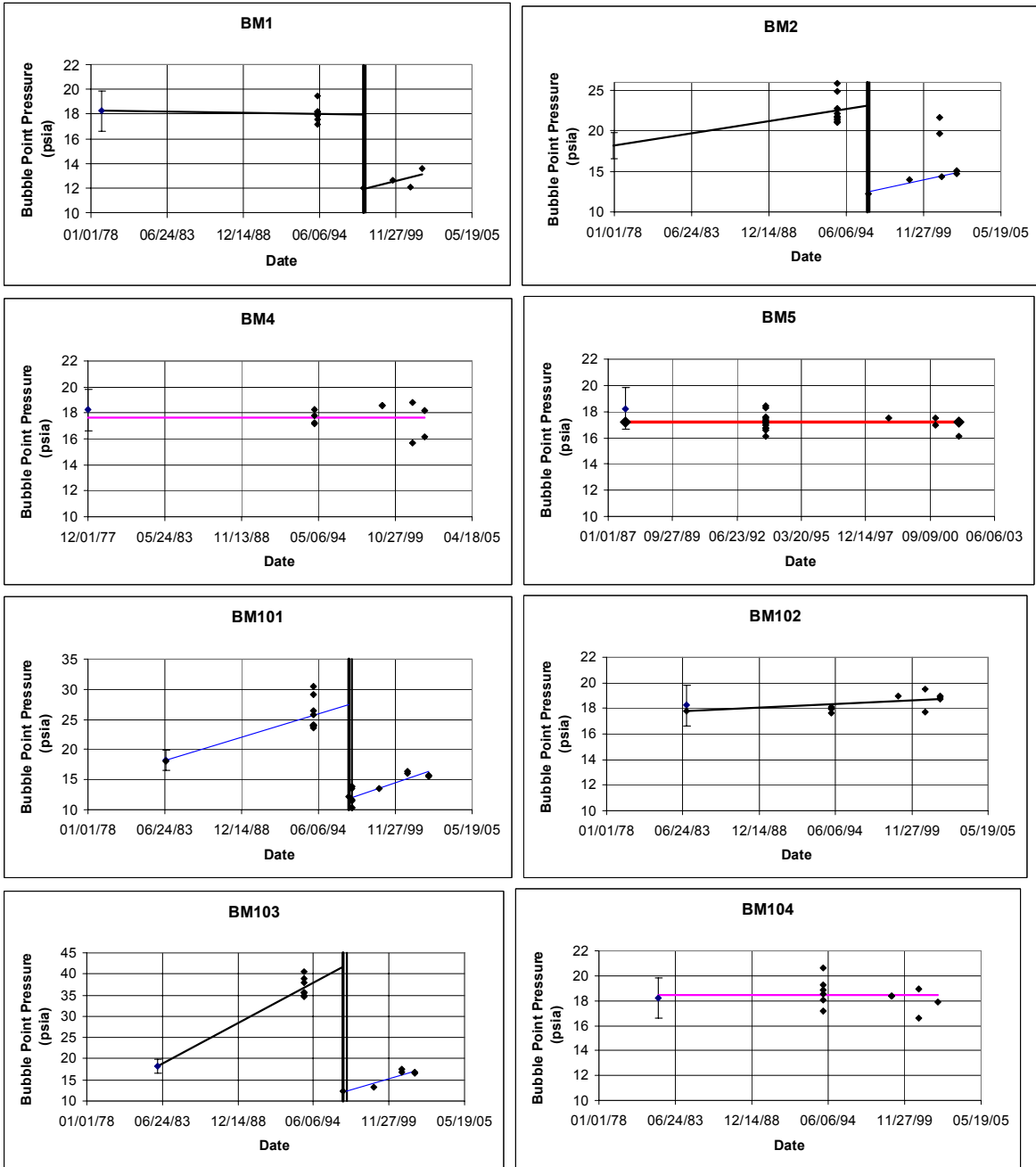
At Big Hill, positive regain rates are observed in all caverns except BH 110. The vertical bars on these plots designate a degas operation, or in the case of BH111-113, the transfer of Weeks Island oil to the caverns.

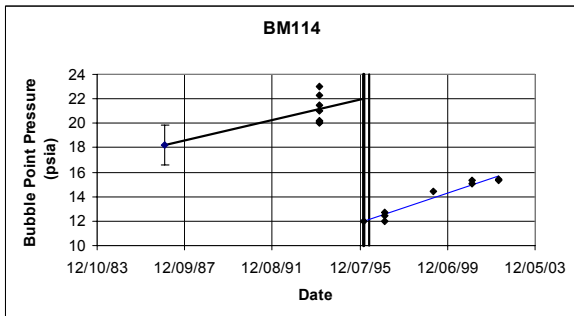
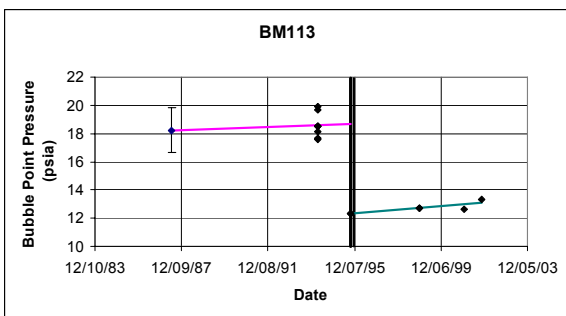
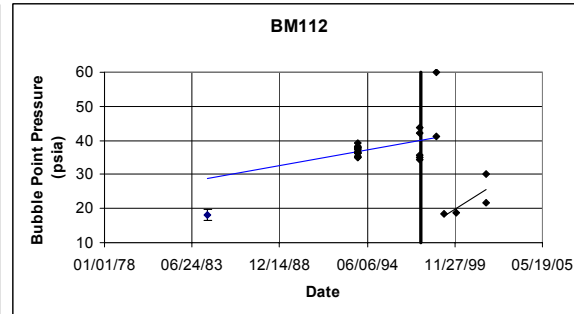
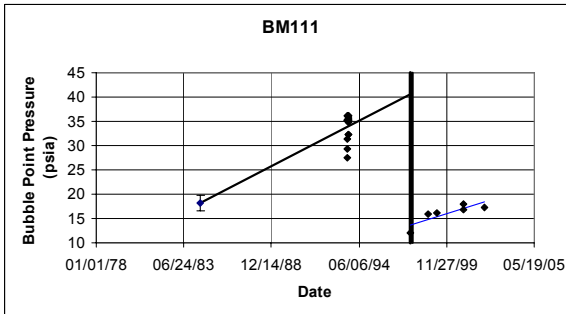
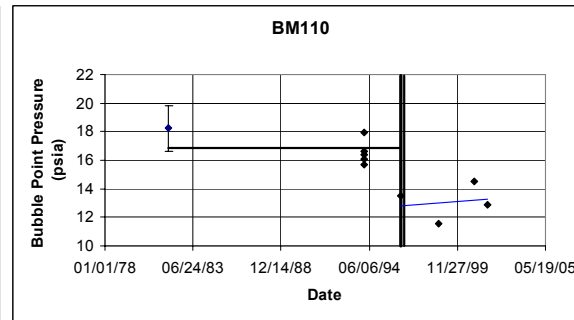
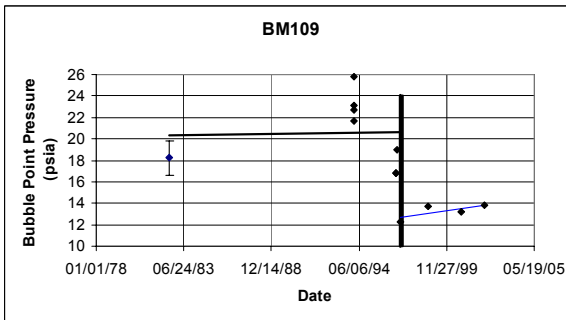
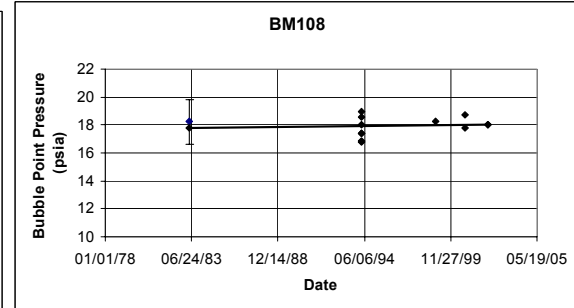
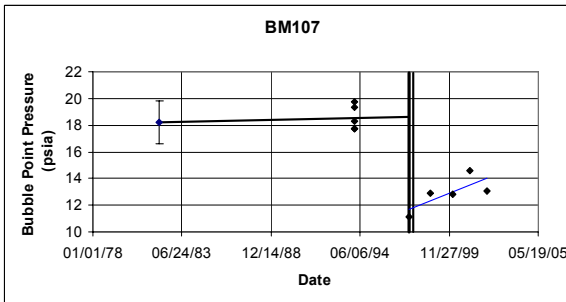
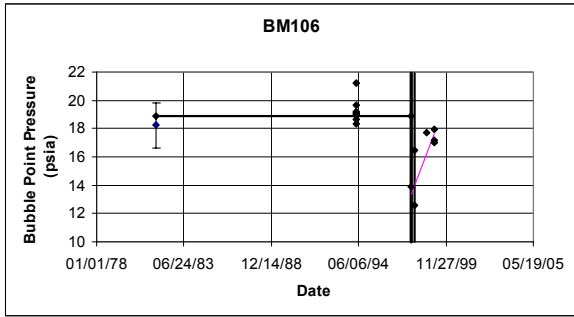
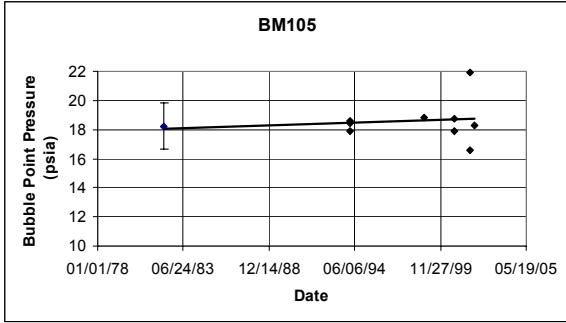


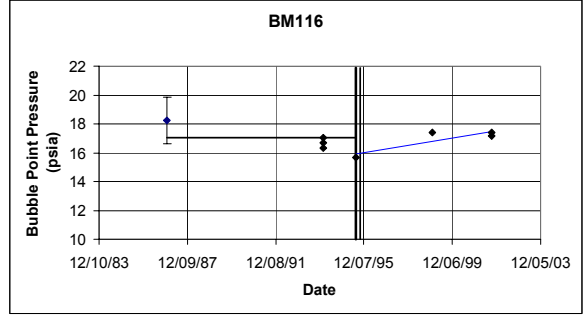
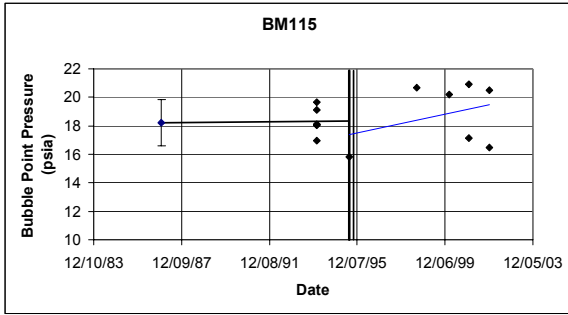




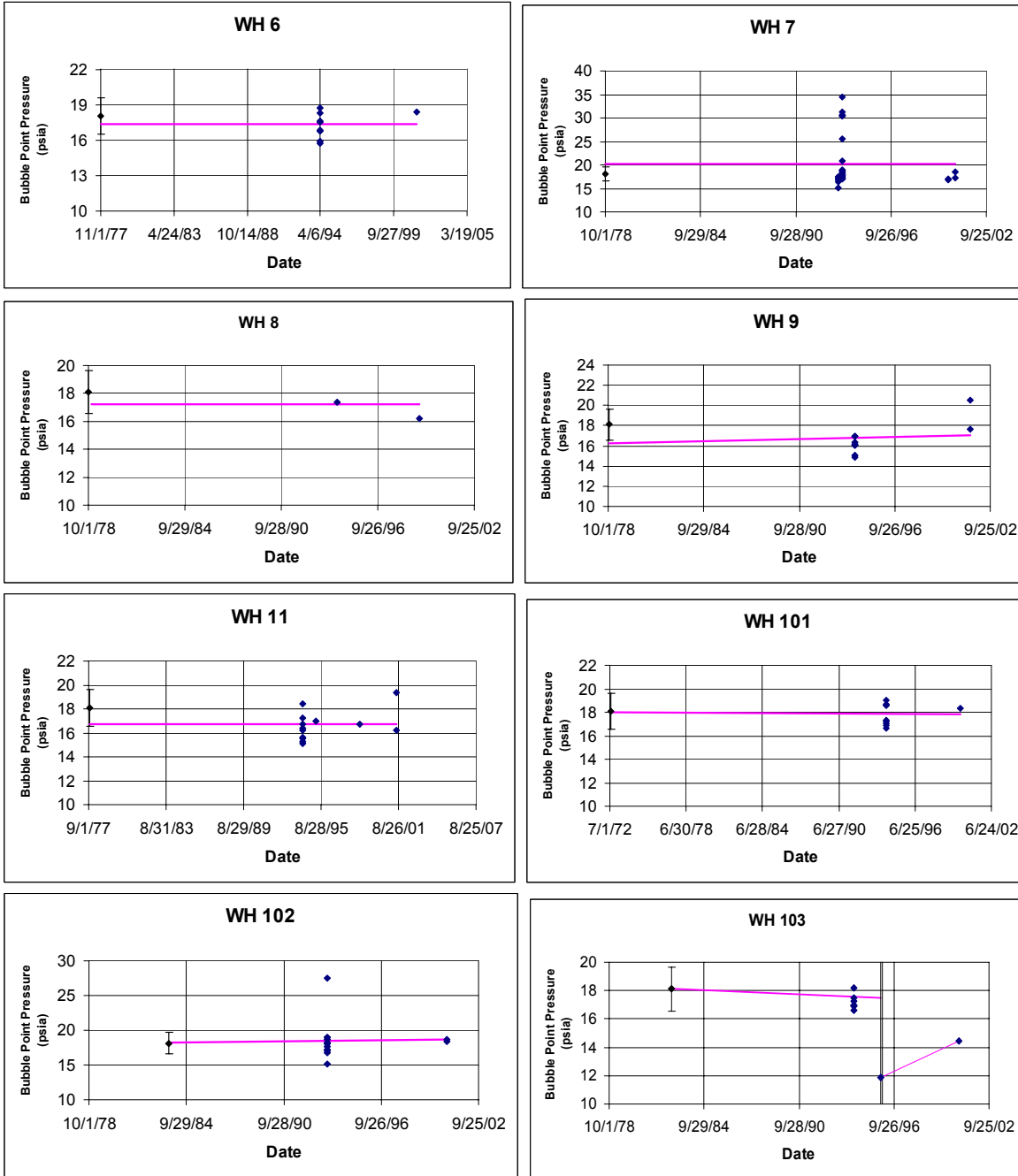
The regain for Bryan Mound caverns is shown at 100 °F in the following graphs. As at Big Hill, positive regain is observed in most caverns.

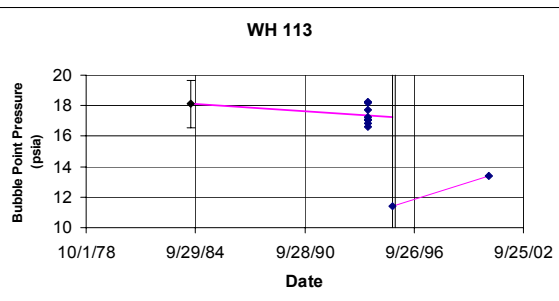
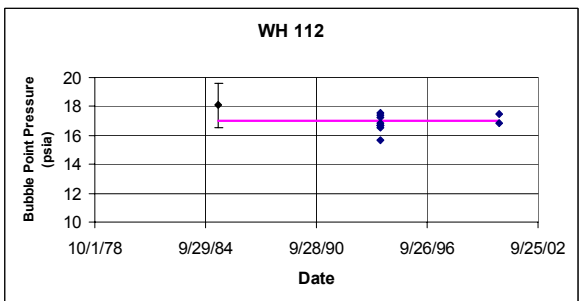
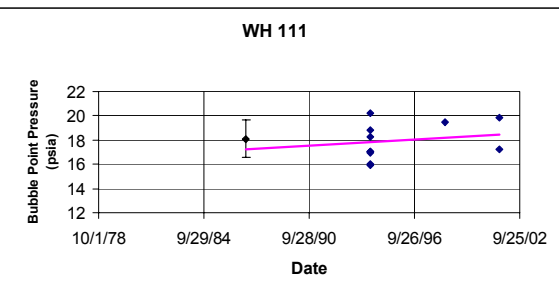
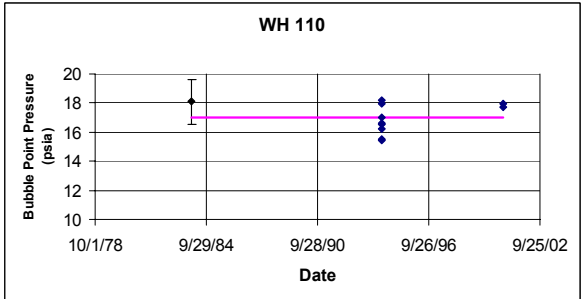
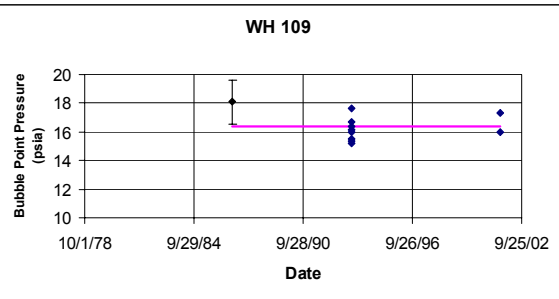
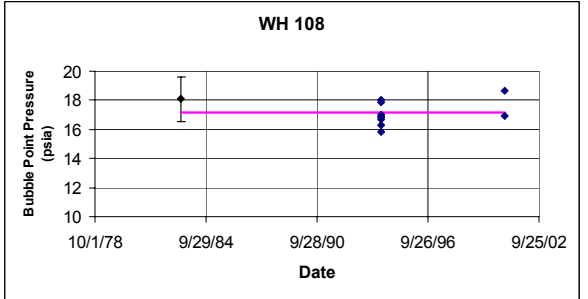
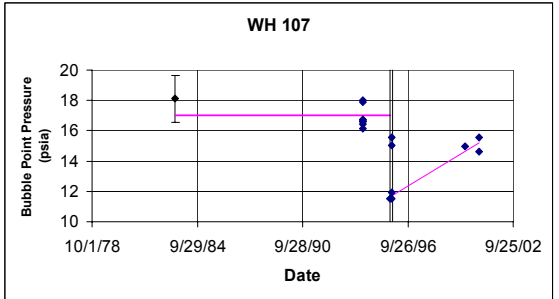
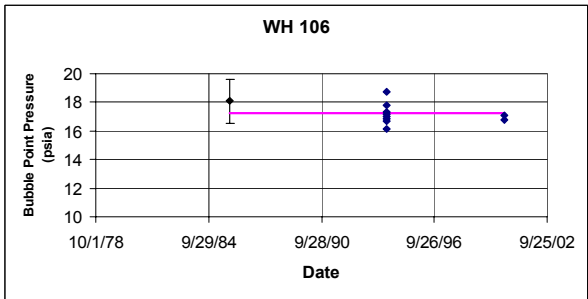
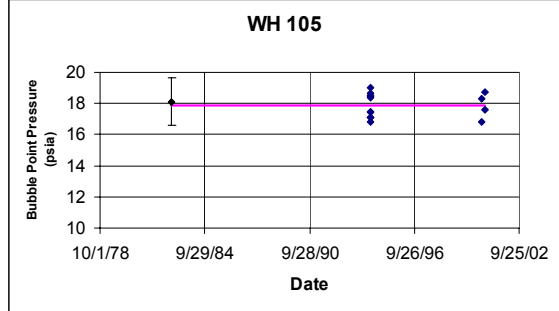
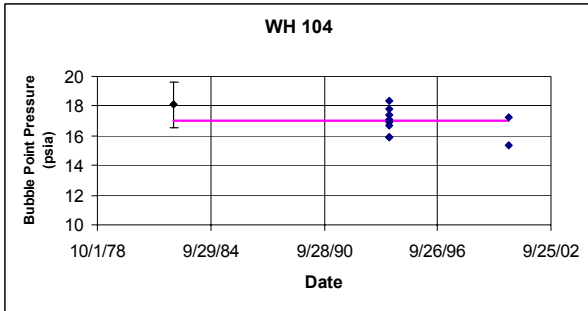


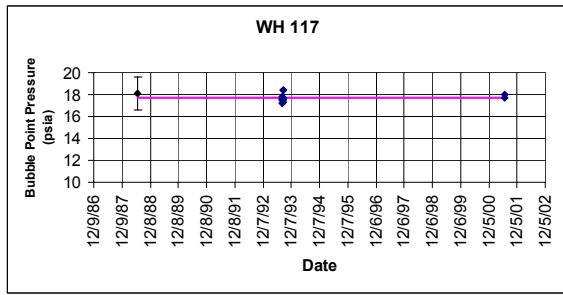
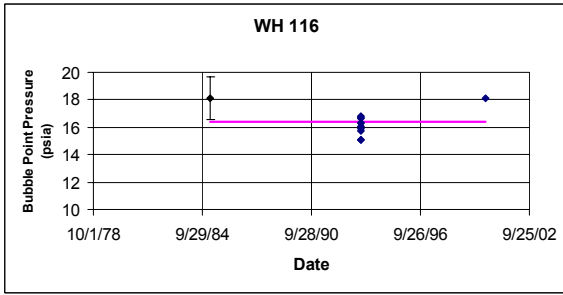
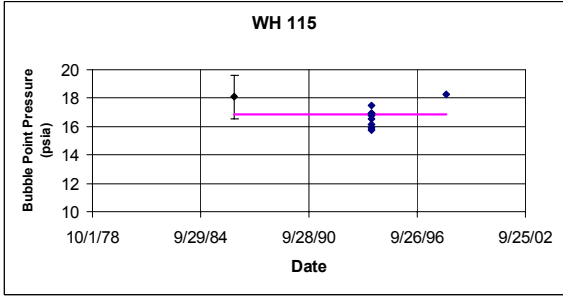
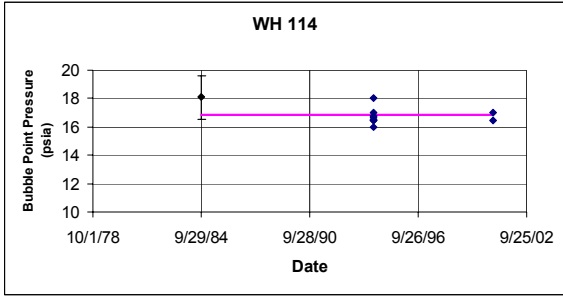




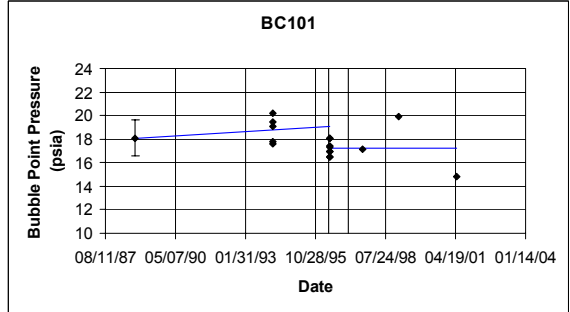
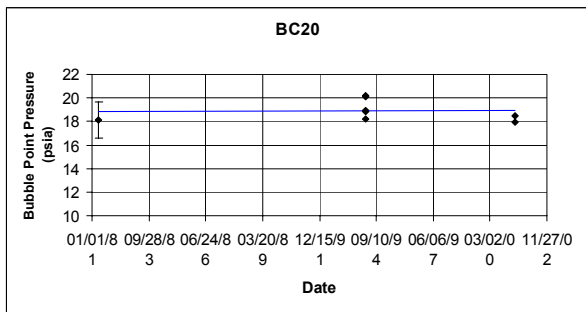
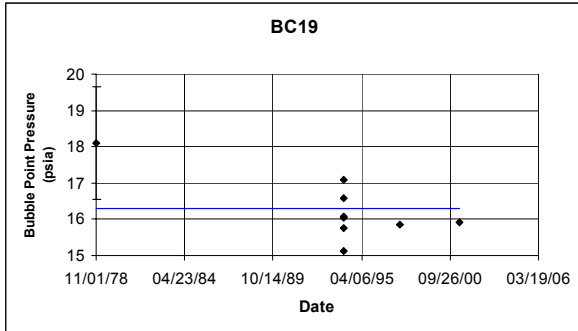
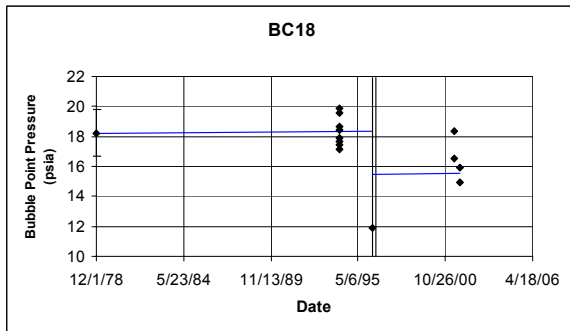
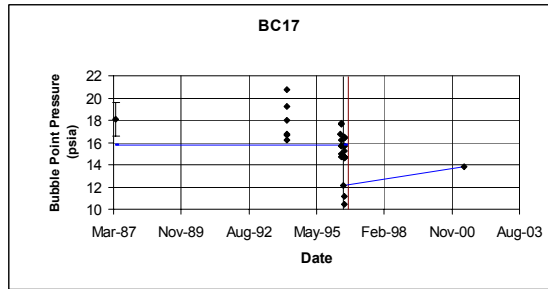
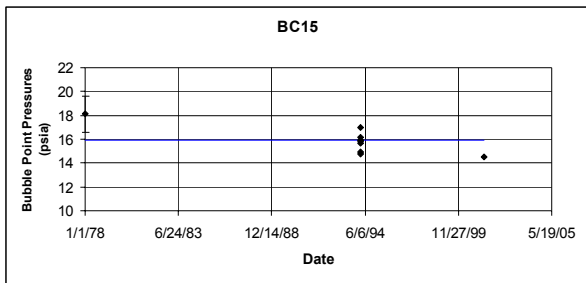
The vapor pressure data for West Hackberry at 100 °F are presented in the following graphs. At this site, there is almost no regain in the caverns. Only degassed caverns (103, 107, and 113) show significant regain.







The regain data for Bayou Choctaw are presented at 100 °F in the following charts. As at West Hackberry, the caverns at Bayou Choctaw have of only a small amount of regain.



Appendix B. Recombined Compositions of Oil Stored in SPR Caverns (Aug. 2002)

The recombined cavern oil compositions, expressed as mole fractions, are presented for all caverns in the tables below. The composition of the combined streams of sweet oil and sour oil are also presented. The primary differences between sweet and sour oil is that the concentration of H₂S is greater for sour oil. It is further observed that the propane content of the sweet streams is approximately 3% while that of the sour stream is approximately 2%. The bubble points and calculated GORs at 100 °F are also presented. The GOR for the sweet streams appear to be greater than the GOR for sour streams while the bubble points are comparable. A negative GOR indicates that the oil vapor pressure is subatmospheric, and the stream may be used as blend stock.

Bayou Choctaw	15	17	18	19	20	101	Sweet	Sour
Ar	0.0000	0.0000	0.0000	0.0000	0.0000	0.0000	0.0000	0.0000
CO	0.0000	0.0000	0.0000	0.0000	0.0000	0.0000	0.0000	0.0000
O2	0.0000	0.0000	0.0000	0.0000	0.0000	0.0000	0.0000	0.0000
H2S	0.0004	0.0009	0.0006	0.0004	0.0000	0.0003	0.0004	0.0005
N2	0.0002	0.0002	0.0001	0.0006	0.0005	0.0004	0.0002	0.0004
CO2	0.0005	0.0009	0.0005	0.0008	0.0006	0.0005	0.0005	0.0006
C1	0.0008	0.0006	0.0003	0.0007	0.0006	0.0008	0.0004	0.0007
C2	0.0042	0.0041	0.0027	0.0035	0.0041	0.0040	0.0032	0.0040
C3	0.0202	0.0189	0.0248	0.0181	0.0302	0.0195	0.0266	0.0193
i-C4	0.0100	0.0093	0.0146	0.0093	0.0151	0.0094	0.0148	0.0096
n-C4	0.0347	0.0332	0.0552	0.0319	0.0456	0.0324	0.0519	0.0332
i-C5	0.0270	0.0250	0.0412	0.0249	0.0328	0.0231	0.0383	0.0252
n-C5	0.0392	0.0383	0.0617	0.0364	0.0396	0.0349	0.0542	0.0374
C6	0.0971	0.0938	0.1956	0.0911	0.0944	0.0884	0.1612	0.0930
C7	0.1810	0.1645	0.6120	0.1680	0.2065	0.1863	0.4745	0.1755
C8 Plus	0.5846	0.6103	-0.0092	0.6143	0.5301	0.5999	0.1737	0.6007
BP (psia)	14.5	13.8	14.9	15.9	18.2	14.8	16.1	14.8
GOR(scf/bbl)	-0.05	-0.27	0.26	0.30	2.23	0.04	0.93	0.00

Big Hill	101	102	103	104	105	106	107	108
Ar	0.0000	0.0000	0.0000	0.0000	0.0000	0.0000	0.0000	0.0000
CO	0.0000	0.0000	0.0000	0.0000	0.0000	0.0000	0.0000	0.0000
O2	0.0000	0.0000	0.0000	0.0000	0.0000	0.0000	0.0000	0.0000
H2S	0.0001	0.0005	0.0000	0.0000	0.0000	0.0007	0.0005	0.0007
N2	0.0003	0.0003	0.0006	0.0006	0.0000	0.0002	0.0002	0.0003
CO2	0.0004	0.0008	0.0004	0.0008	0.0003	0.0009	0.0005	0.0009
C1	0.0005	0.0016	0.0016	0.0022	0.0001	0.0010	0.0010	0.0017
C2	0.0045	0.0031	0.0026	0.0026	0.0018	0.0033	0.0041	0.0040
C3	0.0364	0.0202	0.0420	0.0265	0.0315	0.0182	0.0200	0.0197
i-C4	0.0152	0.0104	0.0114	0.0132	0.0159	0.0088	0.0103	0.0098
n-C4	0.0543	0.0408	0.0425	0.0463	0.0650	0.0332	0.0347	0.0349
i-C5	0.0320	0.0311	0.0263	0.0315	0.0426	0.0250	0.0270	0.0264
n-C5	0.0463	0.0409	0.0389	0.0421	0.0641	0.0393	0.0401	0.0408
C6	0.0905	0.0977	0.0776	0.0902	0.0676	0.0927	0.0935	0.0952
C7	0.2281	0.2999	0.1987	0.2325	0.3259	0.1571	0.1596	0.1638
C8 Plus	0.4912	0.4526	0.5575	0.5114	0.3851	0.6196	0.6085	0.6019
BP (psia)	18.3	17.5	22.0	22.5	13.8	13.7	14.5	17.6
GOR(scf/bbl)	3.96	1.26	4.98	3.82	-0.76	-0.31	-0.08	1.11
Big Hill	109	110	111	112	113	114	Sweet	Sour
Ar	0.0000	0.0000	0.0000	0.0000	0.0000	0.0000	0.0000	0.0000
CO	0.0000	0.0000	0.0000	0.0000	0.0000	0.0000	0.0000	0.0000
O2	0.0000	0.0000	0.0000	0.0000	0.0000	0.0000	0.0000	0.0000
H2S	0.0003	0.0007	0.0002	0.0003	0.0000	0.0000	0.0002	0.0004
N2	0.0000	0.0001	0.0006	0.0003	0.0009	0.0008	0.0002	0.0003
CO2	0.0008	0.0011	0.0005	0.0012	0.0011	0.0013	0.0005	0.0009
C1	0.0005	0.0013	0.0007	0.0009	0.0009	0.0027	0.0009	0.0010
C2	0.0035	0.0041	0.0030	0.0036	0.0035	0.0031	0.0028	0.0036
C3	0.0232	0.0265	0.0245	0.0237	0.0173	0.0172	0.0291	0.0215
i-C4	0.0128	0.0168	0.0119	0.0119	0.0083	0.0108	0.0136	0.0113
n-C4	0.0471	0.0389	0.0404	0.0437	0.0293	0.0343	0.0528	0.0377
i-C5	0.0369	0.0269	0.0293	0.0276	0.0196	0.0288	0.0354	0.0272
n-C5	0.0566	0.0381	0.0433	0.0403	0.0285	0.0405	0.0508	0.0407
C6	0.0660	0.0799	0.1079	0.1046	0.0372	0.0895	0.0830	0.0841
C7	0.3011	0.1898	0.2306	0.2339	0.0678	0.2220	0.2858	0.1864
C8 Plus	0.4511	0.5760	0.5071	0.5079	0.7857	0.5488	0.4449	0.5848
BP (psia)	13.7	16.5	17.4	16.6	18.1	23.7	16.8	16.0
GOR(scf/bbl)	-0.63	1.31	0.90	0.85	0.67	2.82	1.33	0.47

Bryan Mound											
Ar	0.0000	0.0000	0.0000	0.0000	0.0000	0.0000	0.0000	0.0000	0.0000	0.0000	0.0000
CO	0.0000	0.0000	0.0000	0.0000	0.0000	0.0000	0.0000	0.0000	0.0000	0.0000	0.0000
O2	0.0000	0.0000	0.0000	0.0000	0.0000	0.0000	0.0000	0.0000	0.0000	0.0000	0.0000
H2S	0.0009	0.0000	0.0000	0.0021	0.0018	0.0013	0.0007	0.0010	0.0010	0.0009	0.0006
N2	0.0001	0.0000	0.0004	0.0001	0.0001	0.0005	0.0006	0.0001	0.0003	0.0002	0.0001
CO2	0.0005	0.0003	0.0006	0.0013	0.0006	0.0009	0.0007	0.0005	0.0006	0.0010	0.0007
C1	0.0007	0.0003	0.0006	0.0015	0.0007	0.0016	0.0010	0.0009	0.0016	0.0019	0.0005
C2	0.0035	0.0016	0.0040	0.0055	0.0033	0.0043	0.0035	0.0044	0.0049	0.0052	0.0023
C3	0.0209	0.0325	0.0299	0.0210	0.0238	0.0184	0.0172	0.0265	0.0206	0.0215	0.0209
i-C4	0.0114	0.0194	0.0164	0.0105	0.0146	0.0092	0.0082	0.0150	0.0104	0.0078	0.0132
n-C4	0.0410	0.0671	0.0539	0.0360	0.0546	0.0332	0.0306	0.0559	0.0371	0.0307	0.0503
i-C5	0.0334	0.0455	0.0317	0.0283	0.0461	0.0257	0.0223	0.0446	0.0290	0.0179	0.0400
n-C5	0.0518	0.0640	0.0455	0.0435	0.0706	0.0396	0.0347	0.0681	0.0440	0.0279	0.0611
C6	0.1375	0.0689	0.0870	0.0644	0.0804	0.0770	0.0811	0.0788	0.0803	0.0248	0.0665
C7	0.1895	0.3050	0.3994	0.2426	0.3392	0.1907	0.1250	0.3506	0.2488	0.0992	0.2794
C8 Plus	0.5089	0.3954	0.3305	0.5431	0.3644	0.5977	0.6743	0.3537	0.5213	0.7608	0.4644
BP (psia)	13.6	14.9	18.2	17.3	15.6	18.9	16.8	17.9	18.3	17.4	13.1
GOR(scfb/bbl)	-0.55	0.50	2.73	1.73	-1.31	1.50	0.48	5.76	1.68	0.91	-2.44
Bryan Mound	108	109	110	111	112	113	114	115	116	Sweet	Sour
Ar	0.0000	0.0000	0.0000	0.0000	0.0000	0.0000	0.0000	0.0000	0.0000	0.0000	0.0000
CO	0.0000	0.0000	0.0000	0.0000	0.0000	0.0000	0.0000	0.0000	0.0000	0.0000	0.0000
O2	0.0000	0.0000	0.0000	0.0000	0.0000	0.0000	0.0000	0.0000	0.0000	0.0000	0.0000
H2S	0.0008	0.0009	0.0017	0.0011	0.0035	0.0000	0.0003	0.0000	0.0006	0.0002	0.0013
N2	0.0001	0.0000	0.0000	0.0000	0.0001	0.0000	0.0000	0.0004	0.0001	0.0002	0.0002
CO2	0.0005	0.0005	0.0005	0.0007	0.0023	0.0003	0.0003	0.0007	0.0005	0.0006	0.0008
C1	0.0010	0.0006	0.0006	0.0010	0.0027	0.0002	0.0005	0.0017	0.0007	0.0008	0.0011
C2	0.0047	0.0028	0.0032	0.0038	0.0095	0.0017	0.0022	0.0038	0.0029	0.0033	0.0042
C3	0.0280	0.0227	0.0205	0.0237	0.0360	0.0289	0.0305	0.0295	0.0297	0.0292	0.0219
i-C4	0.0162	0.0135	0.0112	0.0147	0.0179	0.0175	0.0204	0.0149	0.0203	0.0168	0.0121
n-C4	0.0609	0.0499	0.0409	0.0548	0.0612	0.0587	0.0667	0.0483	0.0712	0.0565	0.0441
i-C5	0.0481	0.0401	0.0344	0.0449	0.0478	0.0361	0.0480	0.0301	0.0462	0.0359	0.0352
n-C5	0.0724	0.0613	0.0540	0.0687	0.0732	0.0541	0.0630	0.0416	0.0650	0.0507	0.0540
C6	0.0787	0.0734	0.1202	0.0778	0.1076	0.1315	0.0698	0.0770	0.1282	0.0855	0.0802
C7	0.3500	0.3395	0.1392	0.3332	0.4027	0.1672	0.2907	0.2916	0.1182	0.2673	0.2593
C8 Plus	0.3387	0.3947	0.5737	0.3754	0.2354	0.5037	0.4075	0.4604	0.5164	0.4530	0.4857
BP (psia)	18.0	13.8	12.9	17.2	30.0	13.3	15.4	20.5	17.4	17.2	16.5
GOR(scfb/bbl)	4.77	-0.57	-0.84	3.20	27.41	-0.85	1.10	3.78	4.18	2.15	1.36

West Hackberry	6	7	8	9	11	101	102	103	104	105	106	107
Ar	0.0000	0.0000	0.0000	0.0000	0.0000	0.0000	0.0000	0.0000	0.0000	0.0000	0.0000	0.0000
CO	0.0000	0.0000	0.0000	0.0000	0.0000	0.0000	0.0000	0.0000	0.0000	0.0000	0.0000	0.0000
O2	0.0000	0.0000	0.0000	0.0000	0.0000	0.0000	0.0000	0.0000	0.0000	0.0000	0.0000	0.0000
H2S	0.0005	0.0002	0.0003	0.0010	0.0005	0.0000	0.0000	0.0000	0.0000	0.0000	0.0016	0.0000
N2	0.0009	0.0006	0.0005	0.0006	0.0007	0.0007	0.0005	0.0002	0.0006	0.0006	0.0004	0.0003
CO2	0.0012	0.0004	0.0004	0.0006	0.0005	0.0007	0.0003	0.0004	0.0004	0.0004	0.0004	0.0003
C1	0.0006	0.0004	0.0010	0.0014	0.0009	0.0005	0.0001	0.0001	0.0003	0.0003	0.0009	0.0002
C2	0.0023	0.0022	0.0039	0.0041	0.0038	0.0035	0.0024	0.0003	0.0028	0.0031	0.0043	0.0021
C3	0.0189	0.0292	0.0188	0.0197	0.0198	0.0292	0.0295	0.0305	0.0266	0.0295	0.0210	0.0296
i-C4	0.0093	0.0146	0.0094	0.0099	0.0102	0.0141	0.0145	0.0161	0.0124	0.0144	0.0108	0.0144
n-C4	0.0412	0.0516	0.0348	0.0373	0.0370	0.0494	0.0544	0.0573	0.0464	0.0527	0.0385	0.0534
i-C5	0.0299	0.0344	0.0243	0.0284	0.0275	0.0293	0.0356	0.0460	0.0305	0.0347	0.0290	0.0348
n-C5	0.0501	0.0486	0.0364	0.0444	0.0412	0.0409	0.0512	0.0709	0.0446	0.0500	0.0439	0.0507
C6	0.1080	0.1089	0.0555	0.1065	0.0983	0.0388	0.1145	0.1865	0.0815	0.1115	0.0973	0.1116
C7	0.1642	0.1952	0.1715	0.1764	0.1697	0.1377	0.3092	0.3268	0.2310	0.2189	0.2022	0.1925
C8 Plus	0.5730	0.5136	0.6431	0.5697	0.5900	0.6553	0.3877	0.2649	0.5229	0.4838	0.5496	0.5101
BP (psia)	18.4	17.9	16.2	19.1	17.8	18.3	18.5	14.4	16.3	18.2	17.0	15.1
GOR(scF/bbl)	0.92	1.41	0.43	1.53	0.89	1.48	1.37	-0.16	0.55	1.71	0.83	0.15
West Hackberry	108	109	110	111	112	113	114	115	116	117	Sweet	Sour
Ar	0.0000	0.0000	0.0000	0.0000	0.0000	0.0000	0.0000	0.0000	0.0000	0.0000	0.0000	0.0000
CO	0.0000	0.0000	0.0000	0.0000	0.0000	0.0000	0.0000	0.0000	0.0000	0.0000	0.0000	0.0000
O2	0.0000	0.0000	0.0000	0.0000	0.0000	0.0000	0.0000	0.0001	0.0000	0.0000	0.0000	0.0000
H2S	0.0000	0.0008	0.0000	0.0008	0.0023	0.0000	0.0025	0.0013	0.0001	0.0015	0.0000	0.0012
N2	0.0005	0.0003	0.0007	0.0007	0.0004	0.0002	0.0003	0.0004	0.0006	0.0003	0.0005	0.0005
CO2	0.0004	0.0007	0.0004	0.0007	0.0005	0.0003	0.0004	0.0007	0.0006	0.0007	0.0004	0.0006
C1	0.0004	0.0011	0.0004	0.0011	0.0008	0.0001	0.0007	0.0011	0.0002	0.0014	0.0003	0.0010
C2	0.0009	0.0044	0.0027	0.0039	0.0042	0.0004	0.0040	0.0050	0.0023	0.0054	0.0021	0.0042
C3	0.0299	0.0214	0.0275	0.0202	0.0224	0.0285	0.0231	0.0231	0.0326	0.0209	0.0293	0.0208
i-C4	0.0157	0.0104	0.0129	0.0096	0.0114	0.0150	0.0127	0.0111	0.0142	0.0095	0.0144	0.0104
n-C4	0.0557	0.0358	0.0503	0.0361	0.0407	0.0536	0.0451	0.0417	0.0529	0.0350	0.0523	0.0383
i-C5	0.0446	0.0277	0.0341	0.0263	0.0315	0.0430	0.0335	0.0296	0.0329	0.0251	0.0359	0.0283
n-C5	0.0689	0.0406	0.0501	0.0412	0.0466	0.0664	0.0509	0.0445	0.0484	0.0408	0.0528	0.0434
C6	0.1806	0.1016	0.1067	0.0984	0.1058	0.1746	0.1370	0.0645	0.1026	0.0952	0.1168	0.0965
C7	0.3163	0.1745	0.1612	0.1591	0.2064	0.3068	0.0613	0.1755	0.1862	0.1618	0.2333	0.1657
C8 Plus	0.2862	0.5807	0.5530	0.6020	0.5271	0.3112	0.6284	0.6015	0.5264	0.6024	0.4618	0.5892
BP (psia)	17.8	16.6	17.8	18.5	17.2	13.4	16.7	18.3	18.1	17.9	17.0	17.6
GOR(scF/bbl)	1.86	0.86	1.27	1.20	1.12	-0.54	1.05	1.67	1.56	1.47	1.01	1.08

References

Bauer, S. J., "Comments on Permeability Values Used by B. L. Ehgartner for Study of Transient Gas Flow into an SPR Cavern," Sandia National Laboratories Memorandum to File, June 9, 1993.

Bowker, A. H., G. J. Leiberan, Engineering Statistics, Prentice Hall, Englewood Cliffs, NJ, 1972.

Cunningham, R. E., and R. J. J. Williams, Diffusion of Gases and Porous Media, Plenum Press, New York, 1980.

DynMcDermott, "Bryan Mound Gassy Oil Tank Test Report," SPR publication BME-7000.80A0, New Orleans, LA [1993].

Ehgartner, B. L., "Transient Gas Flow Simulation for A SPR Cavern," Sandia National Laboratories Memorandum to J. K. Linn, May 5, 1993.

Ehgartner, B. L., J. T. Neal, and T. E. Hinkebein, Gas Releases from Salt, SAND 98-1354, Albuquerque, June, 1998.

Einfeld, W., "Flammable Gas Modeling Assessment," Sandia National Laboratories Memorandum to T. Hinkebein and R. Matalucci, Sept. 7, 1993.

Hinkebein, T. E., "Plume Analyses of H₂S, Benzene and Total Hydrocarbon Emissions Using the ISCST Gaussian Dispersion Code," Sandia National Laboratories Memorandum to L. J. Rousseau, Feb. 15, 1994.

Hinkebein, T. E. et al., Gas Intrusion into SPR Caverns, Sandia Report 94-0023, Sandia National Laboratories, Albuquerque, NM [1995].

Iannacchione, A.T., Finfinger, G. L., Kohler, T. M. and Hyman, D. M., "Investigation of Methane Emissions from an Advancing Face in the Belle Isle Domal Salt Mine," Bureau of Mines Report PB83-157834, 1982.

Mickley, H. S., T. K. Sherwood, C. E. Reed, Applied Mathemaics in Chemical Engineering, McGraw Hill, New York, 1957.

Reid, R. C., J. M. Prausnitz, B. E. Poling, The Properties of Gases and Liquids, McGraw-Hill, New York, [1987]

Stormont, J.C., "Mechanisms of Gas Production to SPR Caverns," Informal Paper, Aug. 15, 2002.

U.S. Environmental Protection Agency, "Industrial Source Complex, Short Term," ISCST3 Model, Version 4.5i, Office of Air Quality Planning and Standards, Emissions, Monitoring and Analysis Division, Research Triangle Park, NC, [2000]

Intentionally Left Blank

DISTRIBUTION:

U.S. DOE SPR PMO (13)
900 Commerce Road East
New Orleans, LA 70123
Attn: Wayne Elias(10)
TDCS (2)

U.S. Department of Energy (4)
Strategic Petroleum Reserve
1000 Independence Avenue SW
Washington, D.C. 20585
Attn:
D.F. Johnson, FE 421
H.N. Giles, FE 423 (3)

SANDIA INTERNAL

MS 0701 P.B. Davies, 6100
MS 0706 R.E. Finley, 6113 (10)
MS 0706 S.J. Bauer, 6113
MS 0706 B.L. Ehgartner, 6113
MS 0706 T.E. Hinkebein, 6113 (10)
MS 0706 B.L. Levin, 6113
MS 0706 D.E. Munson, 6113
MS 0706 C.A. Rautman, 6113
MS 0706 A.R. Sattler, 6113
MS 0706 S.W. Webb, 6131
MS 9018 Central Tech. Files, 8945-1
MS 0899 Technical Library, 9616 (2)
MS 0612 Review and Approval Desk, 9612
For DOE/OSTI